A TWO-DIMENSIONAL OMEGA EQUATION FOR THE 1000-700 MB LAYER WITH DIABATIC HEATING

PETER S. FERRENTINO

A TWO-DIMENSIONAL OMEGA EQUATION FOR THE 1000-700 MB LAYER WITH DIABATIC HEATING

by

Peter S. Ferrentino
Lieutenant, United States Navy

Submitted in partial fulfillment
for the degree of

MASTER OF SCIENCE IN METEOROLOGY

from the

UNITED STATES NAVAL POSTGRADUATE SCHOOL

May 1966

ABSTRACT

A two-dimensional omega equation is derived by combination of the vorticity and thermodynamic equations. The desired omega is then taken to be the logarithmic average in the 1000-700 mb layer. A diabatic term, after Laevastu, for oceanic areas only is included to deduce the empirical temperature and vapor-pressure changes associated with sensible and latent heating in the maritime layers. Over both continental and oceanic areas a frictional vorticity sink is included in order that excessive energy cannot be generated over the ocean. Among other novel features is the use of the Holl static-stability parameter which affords vertical consistency with analyses prepared by Fleet Numerical Weather Facility.

TABLE OF CONTENTS

LIST OF ILLUSTRATIONS

LIST OF SYMBOLS

Scalar Quantities

T	temperature
T_A	surface air temperature
T_D	surface dew-point temperature
T_W	sea water temperature (surface)
T_{WB}	wet-bulb temperature
T_C	condensation level temperature
θ	potential temperature
e_A	surface vapor pressure
e_S	surface saturation vapor pressure
e_W	vapor pressure over water
e_C	condensation level vapor pressure
P	pressure
P_A	surface pressure
P_C	condensation level pressure
Z	height above mean sea level
Z_T	terrain height
D	Z (actual)- Z (standard atmosphere)
η	absolute vorticity
ζ	relative vorticity
f	coriolis force
ω	vertical motion of a pressure surface
ω_{LO}	vertical motion at the lower boundary
ω_F	vertical motion due to frictional effects

ω_T	vertical motion due to terrain effects
σ	stability parameter
σ_H	Holl stability parameter
V	wind speed
V_{10}	10-meter wind speed
m	mass
ρ	density
t	time
C_D	coefficient of drag
$\dot{Q}$	heating rate per unit mass
Q_c	heat flux for the inversion case
α	cross isobar angle
γ_m	moist adiabatic lapse rate

Constants

$\gamma_d = g/C_p$	dry adiabatic lapse rate
γ_D	dew-point lapse rate
R	gas constant for dry air
C_p	specific heat at constant pressure
L	latent heat of vaporization
g	acceleration of gravity

Vector-scaler operators

$\mathbf{V}$	velocity
$\mathbf{V}_{g_0}$	geostrophic wind velocity
∇A	gradient of A
$\nabla^2 A$	Laplacian of A
$J(A,B)$	Jacobian of A and B

1. Introduction

Little practical use has been made of vertical motions, $\omega = dp/dt$, in short-range forecasting due to the complicated and lengthy computations required. Vertical motion computations are usually the by-product of multilevel baroclinic models and single values must be extracted only after going through the entire three-dimensional procedure. In this paper a two-dimensional vertical motion equation is developed using vertically integrated parameters with an assumed vertical motion profile. The layer-mean omega is especially useful for short-range thickness forecasts and the 1000-700 mb layer has been selected for study. Derivation of the ω-equation is similar to that by Thompson [18] except a diabatic heating term providing a mechanism for development over oceanic areas has been included. Due to the empiricisms employed the non-elliptic conditions mentioned by Pedersen [16] do not arise.

2. The Basic Omega Equation

The diagnostic omega equation is derived by standard means from a vorticity equation and a thermodynamic equation which retains the diabatic term. Equation (1) is the time derivative of the first law of thermodynamics in (x, y, p, t) coordinates.

$$\frac{\partial T}{\partial t} + \mathbf{V}\cdot\nabla T + \frac{T}{\theta}\frac{\partial \theta}{\partial p}\omega = \frac{\dot{Q}}{C_p} \qquad (1)$$

Substituting, $T = -\frac{g}{R}\frac{\partial z}{\partial \ln p}$, which comes from the hydrostatic assumption and the ideal gas law; then dividing by, -g/R, yields equation (2).

$$\frac{\partial}{\partial t}\left(\frac{\partial z}{\partial \ln p}\right) + V\cdot\nabla\left(\frac{\partial z}{\partial \ln p}\right) - \frac{RT}{g\theta}\frac{\partial \theta}{\partial p}\omega = -\frac{R\dot{Q}}{gC_p} \qquad (2)$$

Operating on equation (2) with the Laplacian gives the final form of the thermodynamic equation as shown by equation (3).

$$\frac{\partial}{\partial \ln p}\nabla^2\left(\frac{\partial z}{\partial t}\right) + \nabla^2\left(V\cdot\nabla\left(\frac{\partial z}{\partial \ln p}\right)\right) + \frac{1}{pg}\nabla^2\sigma_H\omega = -\frac{R}{gC_p}\nabla^2\dot{Q} \qquad (3)$$

Here, $\sigma_H = -R_p\frac{T}{\theta}\frac{\partial \theta}{\partial p}$, is the Holl stability parameter to be further discussed in section (4).

The vorticity equation in pressure coordinates is shown by equation (4).

$$\frac{\partial \zeta}{\partial t} + V\cdot\nabla(\zeta+f) + \omega\frac{\partial}{\partial p}(\zeta+f) = (\zeta+f)\frac{\partial \omega}{\partial p} + \left(\frac{\partial \omega}{\partial y}\frac{\partial u}{\partial p} - \frac{\partial \omega}{\partial x}\frac{\partial v}{\partial p}\right) \qquad (4)$$

As presented by Thompson [18] and numerous other writers the last term of the left side of (4) is approximately equal to that on the right side, and the two terms are henceforth deleted. Then, a useful form of the vorticity equation is arrived at (equation 5) by making the geostrophic assumption for vorticity and for velocity, $\zeta_g = \frac{g}{f}\nabla^2 z$, $V_g = \frac{g}{f}\nabla z$, and by taking the logarithmic pressure derivative.

$$\frac{\partial}{\partial \ln p}\nabla^2\left(\frac{\partial z}{\partial t}\right)+\frac{\partial}{\partial \ln p}J(z,\eta)-\frac{f\eta}{g}\frac{\partial}{\partial \ln p}\left(\frac{\partial \omega}{\partial p}\right)=0 \qquad (5)$$

Here, $\eta=\zeta_g+f$, is the absolute vorticity. Next subtract (5) from (3), and the result is the omega equation:

$$\nabla^2(\sigma_H\omega)+f\eta p^2\frac{\partial^2\omega}{\partial p^2}=pg\frac{\partial}{\partial \ln p}J(z,\eta)$$
$$-pg\nabla^2\left(V\cdot\nabla\left(\frac{\partial z}{\partial \ln p}\right)\right)-p\frac{R}{c_p}\nabla^2\dot{Q} \qquad (6)$$

3. Vertical Distribution of Pressure and Omega

Instead of the distribution of pressure indexes normally considered, that employed here is given by,

$$\frac{p_n}{p_0}=\frac{p_0}{p_4}\left(2^{-\frac{n}{4}}\right)=2^{-\frac{n}{4}}$$

where n is an arbitrary pressure level. The 1000-500 mb layer is divided into sub-layers as shown by Figure (1). The resultant pressures, while essentially logarithmic, bear values nearly identical to those of the mandatory levels.

4	$P_4 = P_0 2^{-1}$	500.0 mb
3	$P_3 = P_0 2^{-\frac{3}{4}}$	594.6 mb
2	$P_2 = P_0 2^{-\frac{1}{2}}$	707.1 mb
1	$P_1 = P_0 2^{-\frac{1}{4}}$	840.9 mb
0	$P_0 = P_0 2^{0}$	1000.0 mb

Figure 1. Pressure Distribution in the Vertical

The values of $\omega = dp/dt$, the "vertical" velocity in pressure coordinates, is assumed to vary parabolically in the vertical with a profile defined by equation (7), which extends nearly to the 500 mb level.

$$\omega = A\left(\ln\frac{p}{p_0}\right)^2 + B\left(\ln\frac{p}{p_0}\right) \tag{7}$$

For boundary conditions it is assumed that $\omega = 0$ at $p = p_0$ (the kinematic boundary condition at the assumed surface of the earth, p_0). Also for convenience it is assumed that at p_4 $\partial\omega/\partial p = 0$, i.e. that the 500-mb divergence is zero. Then, upon differentiation of equation (7) with the 500-mb divergence taken to be zero, equation (8) results. It should be noted that if the value $(\partial\omega/\partial p) = 0$ is assumed zero at $p = p_3$ the value of B is altered by only 5%.

$$\left(\frac{\partial\omega}{\partial p}\right)_4 = \left[2A\left(\ln\frac{p}{p_0}\right)\frac{\partial}{\partial p}\left(\ln\frac{p}{p_0}\right) + B\frac{\partial}{\partial p}\left(\ln\frac{p}{p_0}\right)\right]_{p=p_4} = 0$$

or, $$2A\left(\ln\frac{p_4}{p_0}\right)\left(\frac{1}{p_4}\right) + B\left(\frac{1}{p_4}\right) = 2A\left(\ln 2^{-1}\right)\left(\frac{1}{p_4}\right) + B\left(\frac{1}{p_4}\right) = 0 \tag{8}$$

Therefore, B=1.3863A, and the omega profile in terms of A is given by equation (9).

$$\omega = A\left[\left(\ln\frac{p}{p_0}\right) + 1.3863\left(\ln\frac{p}{p_0}\right)\right] \tag{9}$$

Since, $\omega_0 = 0$, the ratio between ω_1, and ω_2, defines the omega profile (equation 10) for the 0-2 layer (see Figure 2).

$$\frac{\omega_2}{\omega_1} = \frac{-\frac{1}{2}A\ln 2\left(-\frac{1}{2}\ln 2 + 1.3863\right)}{-\frac{1}{4}A\ln 2\left(-\frac{1}{4}\ln 2 + 1.3863\right)} = 1.7143 \qquad (10)$$

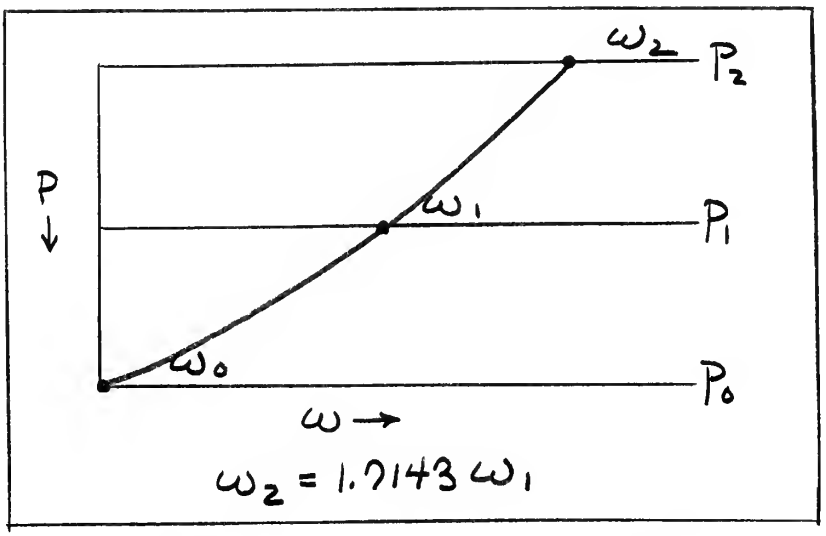

Figure 2. The Omega Profile

For the pressure-range considered (see Figure 2), the layer-logarithmic-mean, $\bar{\omega} = 0.950\omega_1$, so that ω_1, will be used for $\bar{\omega}$. Note finally, the profile assumed here applies only to the large-scale adiabatic, frictionless component of the vertical velocity (that is terrain irregularities are considered absent).

4. Vertical Integration of the Omega Equation

The Holl stability parameter [11] is used since it is one of the vertical-consistency requirements used by FNWF (Fleet Numerical Weather Facility) and this study uses FNWF processed data. The Holl parameter is a modification of the standard stability parameter used here, as shown by equations (11), (12), and (13).

$$\sigma_H = Rp\sigma = -Rp\frac{T\partial\theta}{\theta\partial p} = Rp\left(\frac{RT}{c_p p} - \frac{\partial T}{\partial p}\right) \qquad (11)$$

Letting, $RT = -g\frac{\partial z}{\partial \ln p}$ gives,

$$\sigma_H = -\frac{Rg}{c_p}\frac{\partial z}{\partial \ln p} + R\frac{\partial T}{\partial \ln p} \qquad (12)$$

Equation (12) may now be finite differenced over the 0-2 layer.

$$\bar{\sigma}_H = \frac{R}{\ln\frac{P_0}{P_2}}\left[\frac{R}{c_p}(z_2 - z_0) - (T_0 - T_2)\right] \qquad (13)$$

Equation (13) represents the Holl stability parameter in finite-difference form. In effect, $\bar{\sigma}_H$, by (13) gives the logarithmic-pressure average over the 0-2 layer. This use of $\bar{\sigma}_H$ is compatible with the assumed logarithmic pressure distribution and will be used throughout the analysis which follows.

The omega equation (6) will now be integrated term by term over the isobaric layer (Po, P_2). From (6), one may rewrite the ω-equation as:

$$\overset{(A)}{\nabla^2(\sigma_H\omega)} + \overset{(B)}{f^2 p^2\frac{\partial^2\omega}{\partial p^2}} = \overset{(C)}{pg\frac{\partial}{\partial \ln p}J(z,\zeta)}$$

$$-pg\overset{(D)}{\nabla^2\left(\vec{V}\cdot\nabla\left(\frac{\partial z}{\partial \ln p}\right)\right)} - p\overset{(E)}{\frac{R}{c_p}\nabla^2\dot{Q}}$$

whose parts (A),...., (E) will now be discussed individually.

(A) The first term is approximated by substituting layer mean values: $\nabla^2(\bar{\sigma}_H \omega_1)$, $\omega_1 \doteq \bar{\omega}$

(B) With the mathematical relation, $p^2 \frac{\partial^2 \omega}{\partial p^2} = \frac{\partial^2 \omega}{\partial (\ln p)^2} - \frac{\partial \omega}{\partial \ln p}$, the second term becomes,

$$f\eta_1\left(\frac{\partial^2 \omega}{\partial (\ln p)^2} - \frac{\partial \omega}{\partial \ln p}\right)$$

whose center-finite-differenced form over the 0-2 layer becomes:

$$f\eta_1\left(\frac{\omega_2 - 2\omega_1 + \omega_0}{(\frac{1}{2}\ln P_0/P_2)^2} + \frac{\omega_2 - \omega_0}{\ln P_0/P_2}\right) \qquad (14)$$

Then, using the specified vertical motion profile the relation $\omega_2 = 1.7143\omega_1$, is substituted. However, it is desired to introduce lower boundary effects due to friction and terrain by letting $\omega_0 = \omega_{LO}$, the ω_{LO} term then being predetermined and placed on the forcing function side of the ω-equation. Expression (15) below is the final form of (14) including effects of the lower boundary.

$$\text{Term (B)} \doteq f\eta_1\left(-\frac{0.2857\omega_1}{(\frac{1}{2}\ln P_0/P_2)^2} + \frac{1.7143\omega_1}{\ln P_0/P_2}\right) + f\eta_1\left(\frac{\omega_{LO}}{(\frac{1}{2}\ln P_0/P_2)^2} - \frac{\omega_{LO}}{\ln P_0/P_2}\right) \qquad (15)$$

The lower boundary, ω_{LO} , will be discussed in section (5).

(C) Term (C) in the geostrophic-diagnostic model represents geostrophic advection of absolute vorticity. Averaging in the vertical with respect to the logarithm of pressure leads to equation (16):

$$\frac{1}{\ln\frac{p_0}{p_2}}\int_{p_2}^{p_0}\frac{pg}{\frac{\partial}{\partial\ln p}}\mathbb{J}(z,\eta)\,\Delta\ln p \doteq \frac{p_1 g}{\ln\frac{p_0}{p_2}}\int_{p_2}^{p_0}\frac{\partial}{\partial\ln p}\mathbb{J}(z,\eta)\,\Delta\ln p \qquad (16)$$

The derivation of equation (16) makes use of the mean value theorem, so that $p \doteq p_1$ is represented by p_1 and may be removed from within the integral. Equation (16) then becomes,

$$\frac{p_1 g}{\ln p_0/p_2}\mathbb{J}(z,\eta)\Big|_{p_2}^{p_0} = \frac{p_1 g}{\ln p_0/p_2}\mathbb{J}(z_0,\eta_0) - \frac{p_1 g}{\ln p_0/p_2}\mathbb{J}(z_2,\eta_2) \qquad (17)$$

(D) Term (D) involves the geostrophic advection of thickness within the logarthmic pressure integral. Its value is well approximated by equation (18):

$$\frac{1}{\ln p_0/p_2}\int_{p_2}^{p_0} pg\nabla^2\left(V\cdot\nabla\left(\frac{\partial z}{\partial\ln p}\right)\right)\Delta\ln p = \frac{p_1 g^2}{f\ln p_0/p_2}\nabla^2\int_{p_2}^{p_0}\mathbb{J}\left(z,\frac{\partial z}{\partial\ln p}\right)\Delta\ln p \qquad (18)$$

the right side of which gives equation (19).

$$\frac{p_1 g^2}{f\ln p_0/p_2}\nabla^2\mathbb{J}(z_1,\Delta z) = \frac{p_1 g^2}{f\ln p_0/p_2}\nabla^2\mathbb{J}(z_1, z_2-z_0) \qquad (19)$$

Equation (19) shows that the geostrophic advecting wind may be taken arbitrarily as the level (1) wind.

(E) The diabatic heating term will be vertically integrated in section (6).

The integrated form of the resulting omega equation, subject to the lower and upper boundary conditions (at p_0 and p_4) becomes,

$$\nabla^2(\bar{\sigma}_H\omega_1) + \frac{f\eta_1}{\bar{\sigma}_H}\left(\frac{1.7143\omega_1}{\ln P_0/P_2} - \frac{0.2857\omega_1}{(\frac{1}{2}\ln P_0/P_2)^2}\right)\nabla^2_H =$$

$$-f\eta_1\left(\frac{\omega_{L0}}{(\frac{1}{2}\ln P_0/P_2)^2} - \frac{\omega_{L0}}{\ln P_0/P_2}\right) + \frac{P_1 g}{\ln P_0/P_2}\left(\mathbb{J}(z_0,\eta_0) - \mathbb{J}(z_2,\eta_2)\right)$$

$$+ \frac{P_1 g^2}{f\ln P_0/P_2}\nabla^2\mathbb{J}(z_1, z_2 - z_0) - p\frac{R}{c_p}\nabla^2\dot{Q} \qquad (20)$$

Equation (20) is a Helmholtz-type equation in the variable, $\bar{\sigma}_H\omega_1$. This grouping, $\bar{\sigma}_H\omega_1$, precludes making the usual simplifying approximation of most three-dimensional models. (See for example, Haltiner et al [9]).

$$\nabla^2(\sigma w) = \sigma\nabla^2\omega + \omega\nabla^2\sigma + 2\nabla\sigma\cdot\nabla\omega \doteq \sigma\nabla^2\omega$$

The final solution of equation (20) is to be divided by $\bar{\sigma}_H$ leaving $\omega_1 \doteq \bar{\omega}$, where $\bar{\omega}$ is the mean vertical motion which approximates the 850 mb vertical motion.

5. The Lower Boundary Condition

Vertical motion at the lower boundary ω_{L0}, is the sum of a terrain and a friction term, $\omega_{L0} = \omega_T + \omega_F$.
Here, ω_T, the terrain-effected vertical motion may be described by equation (21) from Berkofski and Bertoni [2].

$$\omega_T = -\rho g\,\mathbb{V}_T\cdot\nabla z_T \qquad (21)$$

Terrain height, z_T, is a smoothed field used operationally by FNWF. The wind velocity at terrain level, $\mathbb{V}_T$, will be arrived at by an objective procedure to be described below.

The friction term ω_F, as shown by equation (22) is a simplified version of Cressman's formula used by Haltiner et al [9].

$$\omega_F = -\rho_T \frac{g}{f} C_D V_T \zeta_T \qquad (22)$$

C_D is the geostrophic drag coefficient derived by Cressman [7], the field of which is in regular use at FNWF. The field of C_D is a set of constants, one for each (ij) grid-point in the Northern Hemisphere.

Since the T subscripts infer application at terrain height, values are used that approximate the particular terrain heights involved. This is done by dividing the 0-2 layer into three terrain-height dependent cases.

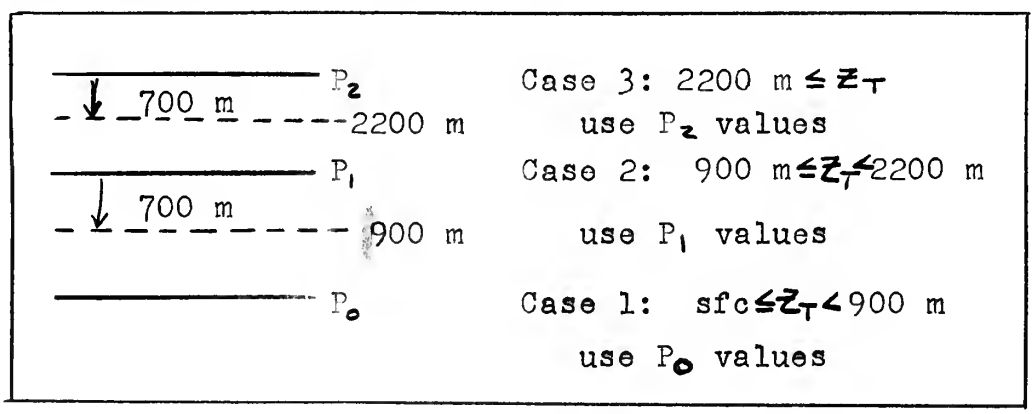

Figure 3. Three Cases of the Lower Boundary

Division of the 0-2 layer as shown by figure (3) is dependent upon the gradient level above terrain, since $|V_T|$ is approximated by some geostrophic wind throughout. As a basis for the selection of the particular geostrophic wind, $|V_g|$, note that the gradient level in a neutral atmosphere occurs at

approximately 700 m above terrain level for a wide range of surface roughness, as shown by Blackadar [3]. Therefore, vertical velocity at the lower boundary is case (1), if the terrain height is 900 m or lower. This values corresponds to a "standard atmosphere" height which is 700m or more below the (1) level, and (0) level parameters are then used to compute the lower boundary. Case (2) is to be used if the terrain height Z_T lies within a gradient-level range of p_1 but not p_2. Case (3) occurs for all terrain heights within 700 m of p_2.

Equation (23) is the terrain-induced vertical velocity at the lower boundary after application of the geostrophic assumption.

$$(\omega_{LO})_n = -\rho_n \frac{g^2}{f} \mathbb{J}(D_n, Z_T) - \rho_n \frac{g^3}{f^3} C_D \left| \mathbb{K} \times D_n \right| \nabla^2 D_n \quad (23)$$

Here, the n subscript refers to the levels 0, 1, and 2. Densities are standard atmosphere values for the respective levels.

6. The Diabatic Heating Term

Diabatic heating in this model results from an exchange of heat between the sea surface and the atmosphere. The exchange is divided into three cases: neutral, convective, and inversion, the division being dependent upon the sea-air temperature difference, $T_w - T_a$.

The neutral case ($0^\circ C \leq T_w - T_A < 3^\circ C$) results in no net transport of heat across the air-ocean interface and the

diabatic heating term is arbitrarily taken as zero when this condition prevails.

The convective case ($T_w - T_A \geq 3^{\circ}C$) results in a net heating of the atmosphere. The convective atmosphere is assumed to consist of a dry adiabatic lapse rate to the condensation level and a moist adiabatic lapse rate above. This particular model of the convective case is discussed by Burke [5] in his paper on the transformation of cP to mP air. Heat gain by the atmosphere is manifested by a layer-mean temperature gain induced by a one-hour trajectory of surface air over a warmer sea-surface, and the layer temperature change is shown by figure (4).

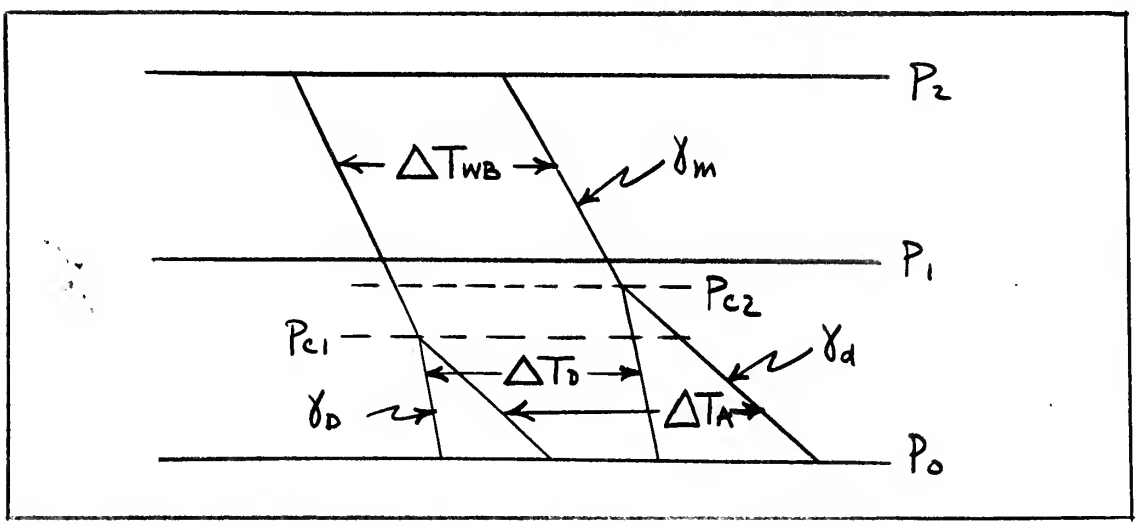

Figure 4. Model of the Convective-Atmosphere Modification

Heating is composed of: (1) sensible heat from the surface to the condensation level and (2) latent heating above this level. This result follows by an analysis of the Burke model and its implications reguarding heat transport. Martin [14] has shown that the large-scale transports of heat have

already been included in those terms of equation (6) in which $\dot{Q}$ does not specifically appear. Thus $\dot{Q}/C_p$, for use in equation (6) is given by the local temperature change.

$$\dot{Q} = C_p \frac{\Delta T}{\Delta t} = \left(C_p \frac{\Delta T_A}{\Delta t} \right)_{SENSIBLE} + \left(C_p \frac{\Delta T_{WB}}{\Delta t} \right)_{LATENT} \qquad (24)$$

Equation (25) is the diabatic heating term (E) referred to in equation (6).

$$-R_p \nabla^2 \frac{\dot{Q}}{C_p} = -R_p \nabla^2 \left[\left(\frac{\Delta T_A}{\Delta t} \right) - \left(\frac{\Delta T_{WB}}{\Delta t} \right) \right] \qquad (25)$$

Integrating logarithmically in the vertical yields the final form of the diabatic term as shown by equation (26).

$$-\frac{R}{\ln P_c/P_2} \nabla^2 \int_{P_2}^{P_c} P \frac{\Delta T_{WB}}{\Delta t} \delta \ln p - \frac{R}{\ln P_A/P_c} \nabla^2 \int_{P_c}^{P_A} P \frac{\Delta T_A}{\Delta t} \delta \ln p$$

$$= -\frac{R}{\ln P_A/P_2} \nabla^2 \left[(P_c - P_2) \frac{\Delta T_{WB}}{\Delta t} + (P_A - P_c) \frac{\Delta T_A}{\Delta t} \right] \qquad (26)$$

In each of equations 24, 25, and 26, the operator $\frac{\Delta}{\Delta t}$ represents the finite-difference version of the local time derivitive, while, P_c, represents a convective-condensation level pressure.

According to the model depicted in figure (4), the modification is largely determined by the static stability which in turn largely depends on $\overline{\sigma_H}$. As an assumed infinite source of heat, the ocean will first modify a thin surface layer of air and then, due to convective activity, will distribute the modification (temperature change) throughout the 0-2 layer. An overestimation of heat exchange should be expected with

this particular process since convection is not instantaneous This overestimation may be partially balanced by heat lost from the top of the 0-2 layer. However, the non-inclusion of a moisture-continuity equation may be more serious in regions of upper ridges.

The inversion case ($T_W - T_A < 0$) or cooling case, where heat is lost from the atmosphere to the ocean is defined by an empiricism from Laevastu [12].

$$Q_c = 3.0\, V_{10} \left(T_W - T_A\right) \text{ gm-cal/cm}^2\text{-24hrs} \qquad (27)$$

Equation (27) represents the heat flux across the 10-meter level. This is an empiricism requiring the 10-meter wind, V_{10}, which will be approximated by making a frictional correction to the 1000 mb geostrophic wind as shown by equation (28):

$$V_{10} = 0.5 \frac{g}{f} \left| \mathbf{k} \times \nabla D_o \right| \qquad (28)$$

The factor 0.5 is due to surface frictional effects and will be discussed in section (7).

Before integrating equation (27) over the 0-2 layer the initial distribution within the layer must be determined. Normally cooling effects due to inversion conditions are confined to a surface layer only several hundred meters thick, however, since the layer mean cooling effect is desired over the entire 0-2 layer it will be assumed that cooling is distributed throughout the 0-2 layer. Thus, dividing equation

(27) by the mass of a column of air extending from the surface pressure P_A to P_2, with total mass, $m = (P_A - P_2)/g$, gives the mean temperature change in a vertical column extending from P_A to P_2 as,

$$\frac{\dot{Q}}{C_p} = \frac{Q_c g}{C_p(P_A - P_2)} \tag{29}$$

Finally we have,

$$-R_p \nabla^2 \frac{\dot{Q}}{C_p} = -\frac{Rg\nabla^2}{C_p \ln\frac{P_A}{P_2}} \int_{P_2}^{P_A} P \frac{Q_c \, \Delta P}{(P_A - P_2)P} = -\frac{Rg}{C_p \ln\frac{P_A}{P_2}} \nabla^2 Q_c \tag{30}$$

which is the final result for the inversion case assuming neglible heat release from fog-droplet condensation.

7. State-Change Parameters for the Convective Case

Air-temperature change and wet-bulb temperature change equations must be derived for use in equation (26). The state-change equations (31) and (32) were initially developed by Mosby [15], Amot [1], and more recently by Boyum [4]. However, in a FNWF study by Carstensen and Laevastu [6] the following best-fit equations were found to give hourly changes with a high degree of skill:

$$\frac{\Delta T_A}{\Delta t} = 0.12(T_w - T_A) - 0.10 - V_{10} \cdot \nabla T_A \quad °C/hr \tag{31}$$

$$\frac{\Delta e_A}{\Delta t} = 0.15(e_w - e_A) - 0.18 - V_{10} \cdot \nabla e_A \quad mb/hr \tag{32}$$

Equation (31) is substituted directly into the sensible-heat term of equation (26) while the wet-bulb temperature change contributes directly to the latent-heat term. In

computing $\frac{\Delta T_{WB}}{\Delta t}$ it is necessary to include the small increment of temperature found by proceeding along a mixing ratio isopleth from P_{c1} to P_{c2} then down a moist adiabat to P_{c1} (see figure 5). Equation (33) shows this relationship.

$$\Delta T_{WB} = \Delta T_D + (\gamma_D - \gamma_m)\Delta z_{pc}, \quad \gamma_D = 1.600 \frac{^{oC}}{km} \qquad (33)$$

Here Δz_{pc} is the one-hour height change of the condensation heights, determined by the height of intersection of the dry adiabat and the mixing ratio isopleth based upon the temperature - dew-point spread at the surface.

$$\Delta z_{pc} = z_{pc2} - z_{pc1} = \left(\frac{T_{A2} - T_{D2}}{\gamma_d - \gamma_D}\right) - \left(\frac{T_{A1} - T_{D1}}{\gamma_d - \gamma_D}\right) \qquad (34)$$

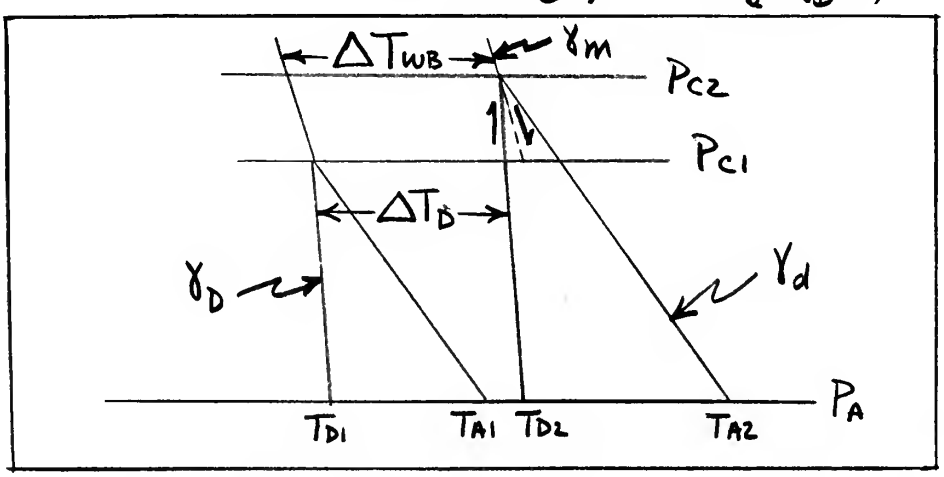

Figure 5. ΔT_{WB} as a Function of ΔT_D

Substituting equation (34) into (33) gives the local rate of change of the wet-bulb temperature as a function of dew-point and air-temperature change.

$$\frac{\Delta T_{WB}}{\Delta t} = \frac{\Delta T_D}{\Delta t} + \left(\frac{\gamma_D - \gamma_m}{\gamma_D - \gamma_d}\right)\left(\frac{\Delta T_A}{\Delta t} - \frac{\Delta T_D}{\Delta t}\right) \qquad (35)$$

The dew-point temperature change ΔT_D is found by taking the time differential of equation (36) below [10],

$$T_A - T_D \doteq \frac{0.622 L}{c_p P}(e_s - e_A) \tag{36}$$

Here, e_s is the saturated vapor pressure and e_A the observed value, both at 10-meters. The finite-difference form of the time differential of dew-point resulting from equation (36) then follows:

$$\frac{\Delta T_D}{\Delta t} \doteq \frac{\Delta T_A}{\Delta t} + \frac{0.622 L}{c_p P}\frac{\Delta e_A}{\Delta t} - \frac{0.622 L}{c_p P}\frac{\Delta e_s}{\Delta t} \tag{37}$$

The vapor pressure change, $\frac{\Delta e_A}{\Delta t}$, is given by equation (32). The time rate of change of saturated vapor pressure, $\frac{\Delta e_s}{\Delta t}$, is calculated using the Clausius - Clapeyron equation:

$$\frac{\Delta e_s}{\Delta t} = \frac{0.622 L e_s}{R T_A^2}\frac{\Delta T_A}{\Delta t} \tag{38}$$

$$e_s = 6.107 \exp\left[\frac{5418.0}{273.16} - \frac{5418.0}{T_A}\right] \tag{39}$$

Equation (39) is an integrated form of the Clausius - Clapyron equation.

There are still some unsolved parameters in the system. The moist adiabatic lapse rate, γ_m, cannot be considered a constant with respect to pressure even in the limited operational range of this study. At the condensation level, P_c, the moist adiabat is calculated from the following [10]:

$$\gamma_m = \gamma_d \left(\frac{P_c + \frac{0.622 L e_c}{R T_c}}{P_c + \frac{(0.622)^2 L^2 e_c}{R T_c^2}} \right) \tag{40}$$

All subscripts C refer to the condensation level.

Condensation parameters of temperature, T_c, and pressure, P_c, are readily calculable from equation (41) and (42) after Edson [8]:

$$T_C = T_A - \frac{\gamma_d}{\gamma_d - \gamma_D} (T_A - T_D) \tag{41}$$

$$P_C = P_A \left(\frac{T_c}{T_A} \right)^{\frac{c_p}{R}} \tag{42}$$

For equation (40), the vapor pressure at the condensation level, e_c, must be calculated. Equation (43), the integrated form of the Clausius - Clapeyron equation may be used since air at the condensation level is saturated, and P_c and T_c are known from (41) and (42).

$$e_c = (6.107) \exp \left[\frac{5418.0}{273.16} - \frac{5418.0}{T_c} \right] \tag{43}$$

In like manner the vapor pressure of the sea surface, e_w, (from equation 32) is calculated since the sea surface is saturated (equation 44). Also, a correction factor of 0.98 is required for salinity effects.

$$e_w = (0.98)(6.107) \exp \left[\frac{5418.0}{273.16} - \frac{5418.0}{T_w} \right] \tag{44}$$

Finally, the advecting wind at 10-meters, $\mathbb{V}_{10}$, must be derived for use in equations (31) and (32). The geostrophic wind at the surface is taken as equal to the 1000 mb geostrophic wind. However, due to frictional interaction with the ocean surface, the geostrophic wind must be reduced in magnitude and rotated to the left, to yield the advecting frictional wind, $\mathbb{V}_{10}$. For the convective case the observed cross-isobar angle at mid-latitudes is approximately 15° [10].

Reduction of the 10-meter wind speed as expressed by the ratio, V/V_{g_0}, where V_{g_0} is the 10-meter geostrophic wind speed, may be obtained from a study by Lettau [13]. By assuming a roughness length of $z_o = 0.1$ cm for oceanic areas, the 10-meter geostrophic wind ratio for neutral conditions is, $V/V_{g_0} = 0.6$. Lettau then allows for stability criteria, and for the convective case a value of $V/V_{g_0} = 0.7$ is arrived at. Similarly, $V/V_{g_0} = 0.5$ for the inversion case.

Advection by the frictional wind is derived by first decomposing the vector advection as shown by equation (45):

$$\mathbb{V} \cdot \nabla T_A = u \frac{\partial T_A}{\partial x} + v \frac{\partial T_A}{\partial y} \tag{45}$$

Then multiplying by 0.7, and rotating the field through the angle $\alpha = 15°$ by a rotational change of coordinates leaves equation (46):

$$\mathbb{V}_{10} \cdot \nabla T_A = 0.7 \left(u_{g_0} \frac{\partial T_A}{\partial x} \cos\alpha - v_{g_0} \frac{\partial T_A}{\partial y} \sin\alpha - v_{g_0} \frac{\partial T_A}{\partial y} \cos\alpha + u_{g_0} \frac{\partial T_A}{\partial x} \sin\alpha \right) \tag{46}$$

Assuming the geostrophic conditions, $u_{g0} = -\frac{g}{f}\frac{\partial z_0}{\partial y}$, $v_{g0} = \frac{g}{f}\frac{\partial z_0}{\partial x}$, equation (46) may be written in its final form as given by equation (47).

$$\mathbf{V}_{10} \cdot \nabla T_A = 0.7 \frac{g}{f} \cos 15^\circ J(z_0, T_A)$$

$$- 0.7 \frac{g}{f} \sin 15^\circ \left(\frac{\partial z_0}{\partial x}\frac{\partial T_A}{\partial y} + \frac{\partial z_0}{\partial y}\frac{\partial T_A}{\partial x} \right) \quad (47)$$

Similarly, equation (48) is derived for the advection of vapor pressure by the 10-meter wind.

$$\mathbf{V}_{10} \cdot \nabla e_A = 0.7 \frac{g}{f} \cos 15^\circ J(z_0, e_A)$$

$$- 0.7 \frac{g}{f} \sin 15^\circ \left(\frac{\partial z_0}{\partial x}\frac{\partial e_A}{\partial y} + \frac{\partial z_0}{\partial y}\frac{\partial e_A}{\partial x} \right) \quad (48)$$

8. Numerical Procedures

All finite-difference operators used are standard centered-differences of the type,

$$\nabla^2 A = \frac{m^2}{d^2}\nabla^2 A \qquad J(A,B) = \frac{m^2}{4d^2} J(A,B)$$

$$\Delta_R A = \frac{m}{2d}\Delta_R A = \frac{m}{2d}\left[(\Delta_x A)^2 + (\Delta_y A)^2 \right]^{\frac{1}{2}}$$

with five-point grids having a mesh distance, d = 381 km at 60° latitude. Here, m is the map factor for polar stereographic projections and d is the grid spacing.

The variables needed for input into the diagnostic omega equation were scaled as follows:

$m = \hat{m}\,.2$ $\qquad$ $p = \hat{p}\,.2^{11}$ mb

$\eta = \hat{\eta}\,.2^{-9}$ sec^{-1} $\qquad$ $e = \hat{e}\,.2^{9}$ mb

$\omega = \hat{\omega}\,.2^{8}$ mb/sec $\qquad$ $\sigma_H = \hat{\sigma}_H\,.2^{35}$ cm^2/sec^2

$\omega_{Lo} = \hat{\omega}_{Lo}\,.2^{8}$ mb/sec $\qquad$ $Z_T = \hat{Z}_T\,.2^{20}$ cm

$D = \hat{D}\,.2^{17}$ cm $\qquad$ $Q = \hat{Q}\,.2^{10}$ gm-cm^2/sec^3

$T = \hat{T}\,.2^{9}$ °C $\qquad$ $f = 1.45842\times10^{-4}\sin\phi$ sec^{-1}

The following physical constants were also needed in the computations of ω. All values of those constants have been expressed in cgs units.

d = 38,1000,000 cm

g = 980.0 cm/sec^2

R = .0287 X 10^7 cm^2/sec^2 - °K

R_v = 0.461 X 10^7 cm^2/sec^2 - °K

C_p = 1.003 X 10^7 cm^2/sec^2 - °K

L = 2500 X 10^7 cm^2/sec^2 - °K

γ_d = 0.9771 X 10^{-4} °C/cm

γ_D = 0.1600 X 10^{-4} °C/cm

ρ_0 = 1.213 X 10^{-3} gm/cm^3

ρ_1 = 1.055 X 10^{-3} gm/cm^3

ρ_2 = 0.919 X 10^{-3} gm/cm^3

The scaled Helmholtz equation, which follows from equation (20), expressed in units of, mb - cm^2/sec^3 , is shown on next page.

$$\nabla^2\left(\hat{\bar{\sigma}}_H\hat{\omega}_1\right) - 4.5873\frac{\hat{f}\hat{\eta}_1 d^2}{\hat{\bar{\sigma}}_H\hat{m}^2}\left(\hat{\bar{\sigma}}_H\hat{\omega}_1\right)\cdot 2^{-46} =$$

$$-30.54\hat{f}\hat{\eta}_1\frac{d^2}{\hat{m}^2}\hat{\omega}_{LO}\cdot 2^{-46} - \frac{g^2\hat{P}_1\hat{m}^2\nabla^2 J\left(\hat{D}_1, \hat{D}_2-\hat{D}_0\right)\cdot 2^4}{f\ln\frac{P_0}{P_2}4d^2}$$

$$+\frac{g\hat{P}_1}{4\ln\frac{P_0}{P_2}}\left[J\left(\hat{D}_0,\hat{\eta}_0\right) - J\left(\hat{D}_2,\hat{\eta}_2\right)\right]\cdot 2^{-24} - pR\nabla^2\frac{\hat{\dot{Q}}}{c_p}\cdot 2^{-43} \qquad (49)$$

All height values have been replaced by D-values, the deviation of the height field from a standard atmosphere height.

The scaled stability parameter is given by equation (50) and is in units of cm^2/sec^2.

$$\hat{\bar{\sigma}}_H = \frac{R}{\ln\frac{P_0}{P_2}}\left\{\frac{g}{c_p}\left[\left(\hat{D}_2-\hat{D}_0\right)\cdot 2^{19}+290000\right] - \left(T_0-T_2\right)2^9\right\}2^{-35} \qquad (50)$$

For computation of the stability parameter D is re-scaled to $D = \hat{D}\ .2^{19}$ to prevent overflow when adding the standard height, $Z_{700}-Z_{1000}$ = 290,000 cm. Stability calculations are based on 1000-700 mb differences and throughout the derivation all gradients and differences at the P_1 and P_2 levels are assumed equal to those at 850 mb and 700 mb respectively.

To prevent computational instability during the numerical Helmholtz solution a minimum value of stability is required.

This value corresponds to a maximum lapse of $\frac{1}{8}\gamma_d$:

$$\left(\hat{T}_0-\hat{T}_2\right)z^9 \leq \frac{2}{8}\frac{g}{c_p}\left[\left(\hat{D}_2-\hat{D}_0\right)\cdot z^{19}+290000\right]$$

Equation (51) is the scaled lower boundary condition in units of mb/sec.

$$\left(\hat{\omega}_{LO}\right)_\eta = -\rho_\eta \frac{g^2\hat{m}^2}{\hat{f}\,4d^2}(10^{-3})\mathcal{J}\left(\hat{D}_\eta,\hat{Z}_T\right)z^{31}$$

$$-\rho_\eta \frac{g^3\hat{m}^3}{\hat{f}^3 2d^3}(10^{-3})C_D\Delta_R\hat{D}_\eta\nabla^2\hat{D}_\eta\cdot z^{29} \qquad (51)$$

Here, the subscript η refers to the terrain-height dependent cases, 1, 2, and 3 explained in section (5). The factor 10^{-3} converts dynes/cm^2 to millibars.

Equations for the diabatic term are computed in terms of heating rates, $\dot{Q}/C_p$, which are assigned to grid points according to the existing grid condition: convective, inversion, or neutral.

Equation (52) shows the scaled heating rate for the convective case.

$$\frac{\hat{\dot{Q}}}{c_p} = \left[\left(\frac{\hat{P}_A-\hat{P}_C}{3600}\right)\frac{\Delta\hat{T}_A}{\Delta t}+\left(\frac{\hat{P}_C-\hat{P}_2}{3600}\right)\frac{\Delta\hat{T}_{WB}}{\Delta t}\right]\cdot z^{10} \qquad (52)$$

The factor, 3600, converts hours to second and heating rate is now in units of mb - °C/sec.

Equation (53) shows the scaled heating rate for the inversion case (a cooling process) also in mb - °C/sec.

$$g\left(\frac{\hat{Q}_c}{C_p}\right) = \frac{g^2 \hat{m}}{\hat{f}^2 d} \frac{(0.5)(0.03)(4.184\times10^7)\Delta_x \hat{D}_o(\hat{T}_w - \hat{T}_A)2^{17}}{K C_p} \quad (53)$$

The factor (4.184×10^7) converts gm-cal/sec to dyne-cm/sec; K = 24 X 3600 which converts 24-hours to seconds; 0.03 replaces 3.0, and permits velocity computation to be made in cm/sec.

Land area grid points are masked and receive heating rate values of zero as do oceanic grid points which satisfy the neutral conditions. The remaining oceanic grid points receive either heating or cooling values depending on the prevailing condition at the point. The diabatic term is then computed and the scaled form in units of mb-cm^2/sec^3 is shown by equation (54).

$$-\frac{R}{\ln\frac{P_o}{P_2}} \nabla^2 \frac{\hat{Q}}{C_p} \cdot 2^{-33} \quad (54)$$

Here, P_o approximates P_A for ease of computation.

Other equations involved in the computation of the diabatic term are scaled as follows:

(1) The air temperature change is units of °C/hr.

$$\frac{\Delta \hat{T}_A}{\Delta t} = 0.12(\hat{T}_w - \hat{T}_A) - (0.10)2^{-9}$$

$$-0.7\frac{g\hat{m}^2}{\hat{f}^4 d^2}\left[\cos 15^\circ J(\hat{z}_o, \hat{T}_A) - \sin 15^\circ\left(\Delta_x \hat{z}_o \Delta_y \hat{T}_A + \Delta_y \hat{z}_o \Delta_x \hat{T}_A\right)\right]2^{19} \quad (55)$$

(2) The dew-point temperature change in units of °C/hr.

$$\frac{\Delta\hat{T}_D}{\Delta t} = \frac{\Delta\hat{T}_A}{\Delta t} + \frac{0.622L}{C_p \hat{P}_A}\left\{0.15(\hat{e}_W - \hat{e}_A) - (0.18)2^{-9}\right.$$

$$- 0.7\frac{g\hat{m}^2}{\hat{f}4d^2}\left[\cos 15^\circ \mathcal{J}(\hat{z}_0, \hat{e}_A) - \sin 15^\circ\left(\Delta_x\hat{z}_0\,\Delta_y\hat{e}_A + \right.\right.$$

$$\left.\left.\left. + \Delta_y\hat{z}_0\,\Delta_x\hat{e}_A\right)\right]2^{19}\right\} 2^{11} - \frac{\left(0.622L^2\hat{e}_S\right)\Delta\hat{T}_A}{C_p\hat{P}_A R_V\left(\hat{T}_A\cdot 2^9 + 273.16\right)^2\Delta t}\,2^{-2} \quad (56)$$

(3) The wet-bulb temperature change in units of °C/hr.

$$\frac{\Delta\hat{T}_{WB}}{\Delta t} = \frac{\Delta\hat{T}_D}{\Delta t} + \left(\frac{\gamma_m - 0.1600}{0.8171}\right)\left(\frac{\Delta\hat{T}_A}{\Delta t} - \frac{\Delta\hat{T}_D}{\Delta t}\right)$$

where,
$$\gamma_m = 0.9771\,\frac{\hat{P}_c\cdot 2^{11} + R\left(\hat{T}_c\cdot 2^9 + 273.16\right)}{\hat{P}_c\cdot 2^{11} + \dfrac{0.622L^2\hat{e}_c\cdot 2^9}{C_p R_V\left(\hat{T}_c\cdot 2^9 + 273.16\right)^2}} \quad (57)$$

(4) The condensation level temperature in units of °C.

$$\hat{T}_C = \hat{T}_A - \left(\frac{0.9771}{0.8171}\right)\left(\hat{T}_A - \hat{T}_D\right) \quad (58)$$

(5) The dew-point temperature in units of °C.

$$\hat{T}_D = \hat{T}_A - \frac{0.622L\left(\hat{e}_S - \hat{e}_A\right)}{C_p\hat{P}_A} \quad (59)$$

(6) The condensation level pressure in units of millibars, $\hat{P}_C = \left(\hat{P}_{C1} + \hat{P}_{C2}\right)/2$

and,
$$\hat{P}_{C1} = \hat{P}_A\left(\frac{\hat{T}_{C1}\cdot 2^9 + 273.16}{\hat{T}_A\cdot 2^9 + 273.16}\right)^{\frac{C_p}{R}} \quad (60)$$

Here $\hat{T}_{C1}$ is computed using values of $\hat{T}_A$ and $\hat{T}_D$ in equation 58.

$$\hat{P}_{C2} = \hat{P}_A\left[\frac{\hat{T}_{C2}\cdot 2^9 + 273.16}{\left(\hat{T}_A + \frac{\Delta\hat{T}_A}{\Delta t}\right)2^9 + 273.16}\right]$$

Here $\hat{T}_{C2}$ is calculated using values of $\hat{T}_{A1} + \Delta\hat{T}_A/\Delta t$ and $\hat{T}_{D1} + \Delta\hat{T}_D/\Delta t$ in equations (58), (59), (55), and (56).

9. The Computer Program

The Control Data Corporation 1604 digital computer was used in this study. It has a core capacity of 32,768 words of 48 bits each. An operational field of 1,977 grid points forming a 51 X 47 octagon inscribed within the 9°N latitude circle was employed. The grid-mesh is 381 km true at 60°N latitude.

Boundary conditions around the octagonal grid were determined by the standard subroutines used. Laplacian, Jacobian, and all other five-point center-difference operations set the grid boundary to zero. The Helmholtz relaxation operation set the edge and the next interior border point to zero.

Equation (49) was solved by a two-dimensional Liebmann relaxation technique wherein the $(n+1)$-iterate for any point is given by.

$$A_{ij}^{n+1} = A_{ij}^{n} + \frac{\lambda}{4}\left[\frac{\nabla^2 A_{ij} - (AB)_{ij} - C_{ij}}{2^{-2}B_{ij} + 1}\right]^n$$

Here, λ is the over-relaxation coefficient and the residual at any step, R_n, is,

$$R_n = \frac{\lambda}{4}\left[\frac{\nabla^2 A_{ij} - (AB)_{ij} - C_{ij}}{2^{-2}B_{ij} + 1}\right]^n$$

The over-relaxation coefficient used was, $\lambda = 1.414$, which allowed convergence in approximately 30 scans over the 1977 point grid using an initial guess field of zero. The convergence criterion is that the iteration ceases when $\epsilon^{(n)}$ defined by $\epsilon^{(n)} \equiv A^{(n+1)} - A^{(n)}$ falls below 3000 mb-cm^2/sec^3. This value corresponds to a vertical velocity of 0.3×10^{-4} mb/sec for a stability of 83×10^6 cm^2/sec^2 (the standard atmosphere stability).

Total computation time was approximately 1 minute and 30 seconds with 23 seconds required for the heating term and 26 seconds for the boundary condition.

Due to the abrupt cut-off criteria used for delineating the three cases of diabatic heating (inversion, convective, neutral) the final $\dot{Q}/c_p$ field was smoothed with a five-point smoother of the form,

$$\bar{A} = A + K\nabla^2 A$$

The smoothing coefficient k is a constant value of (1/8) and the field was smoothed twice. The smoothing operation removed small scale irregularities caused by the cut-off criteria of the heating term but also reduced peak values.

A standard FIWF filtering process followed all operations involving the Laplacian. This process removes all small scale features with wave numbers greater than 15 at latitude 45°.

10. Results and Conclusions

A series of four successive 12-hourly data-sets beginning with the 00Z maps of 28 April 1966 and ending with 12Z, 29 April 1966 were used. Since the only diabatic heating mechanism introduced into this study was that arising by "conduction" from the underlying oceanic surface, the results have been depicted only over the North Atlantic Ocean. This region has a large density of reporting ships and thus the reason for its selection.

The computational omegas and their associated parameters for 00Z 28 April 1966 are contained in figures (6) through (11) which are appended. Of these, not only the diabatic omegas are shown, but also, the additive effect of the diabatic influence as contrasted with adiabatic computations. In figures (12) through (17) only the final-product omegas of this study are shown together with the corresponding FNWF analyzed 850 mb D-fields to serve as identifiers, that is, to indicate qualitative coherency between the vertical motions and the associated motion systems.

In the sequence of figures (6) through (11), it is of interest to note the pattern similarity between comparative adiabatic vertical motion computations, those produced here, and, for the same times, those produced by FNWF, which are based upon the procedure described by Haltiner et al [9]. The magnitude and position of the updraft-centers show a strong similarity with those of FNWF, however, the model described by this paper shows larger downdraft areas extending east-

ward from Newfoundland. This apparent discrepancy may be attributed to the two differing treatments in ω_{Lo} (figures 18 and 19). The ω_{Lo} at the continent-edge essentially becomes the boundary condition for the oceanic computations.

On the other hand, however, one of the major objectives of this study was to test a simplified ω_{Lo} which uses only parameters pertaining to the standard levels of analysis (equation 23). In this connection, the greatest time-consuming aspect of the FNWF ω-computation is that of deriving ω_{Lo}, and associated parameters at terrain height requiring pressure extrapolation. The general similarity in the fields of ω_{Lo} by the two operational procedures which have been discussed is evident by an inspection of figures (18) and (19), and this can perhaps be a justification for continuing the simpler ω_{Lo} computations.

The diabatic effects, which were obtained for the 00Z April 28 synoptic time, depict values of $\dot{Q}/Cp$, so that the large positive center southeast of Newfoundland is realistic with regard to the northerly flow passing over the Gulf Stream. The maximum heating value for the four map periods over the Gulf Stream is $\dot{Q}/Cp = 0.067$ mb - °C/sec, which corresponds to a layer mean heating rate of 0.3 °C/hr for the 1000-700 mb layer. The equivalent thickness change for this layer is approximately 3 meters/hr.

For comparison, Petterssen's values [17] for the 1000-500 mb thickness change during a similar synoptic situation in late March show a maximum value of 6 to 8

meters/hr in the vicinity of the Gulf Stream. These values for sensible and latent heating were computed using flux calculations at the surface based on empiricisms similar to those of Laevastu. It should be noted that heating rates for this time period in late March are indeed greater than late April values.

Finally, with regard to the diabatic term, note that in the area of qualitative verification no significant diabatic cooling values were observed. These areas are limited in extent in winter and spring, but could be of greater synoptic consequence in the summer and fall seasons.

The effect of the diabatic term as it appears on the forcing function side of equation (24) gives rise to figure (11), applicable at approximately 850 mb, but actually representing the layer-mean $\bar{\omega}$. As could be anticipated from the standpoint of heat injection into moving parcels, the change (inclusion of the diabatic term) has been such as to expand the southern rim of the trough which extends towards the southwest from Iceland. Similar aspects of coherency between the resultant ω of this study and the trough movement and development may be traced out, feature by feature as one proceeds through the synoptic sequences. For example, the pronounced trough over the Atlantic has, by 00Z of 29 April, become oriented North-South just east of Greenland. At the same time the updraft cell has taken on this same orientation just west of the same trough, so that the $\bar{\omega}$-field gives some confirmation of the dynamic

processes involved in these map changes.

The model for vertical motion, as presented by this paper, appears to be quite sucessful and future plans involve inclusion of a more realistic frictional term. These more realistically computed omegas (extended to 500 mb) are then to be used for feedback to yield a prognostic z-field, hour-by-hour. The ultimate aim, of course, is to realize a smaller R.M.S. error as the motion systems progress over the ocean.

11. Acknowledgements

The original research for this paper was by Professor Frank L. Martin of the United States Naval Postgraduate School. His assistance and encouragement are gratefully acknowledged. Also, the personnel of Fleet Numerical Weather Facility, especially Mr. Leo C. Clarke, are acknowledged for their invaluable assistance in adapting the model to a computer program.

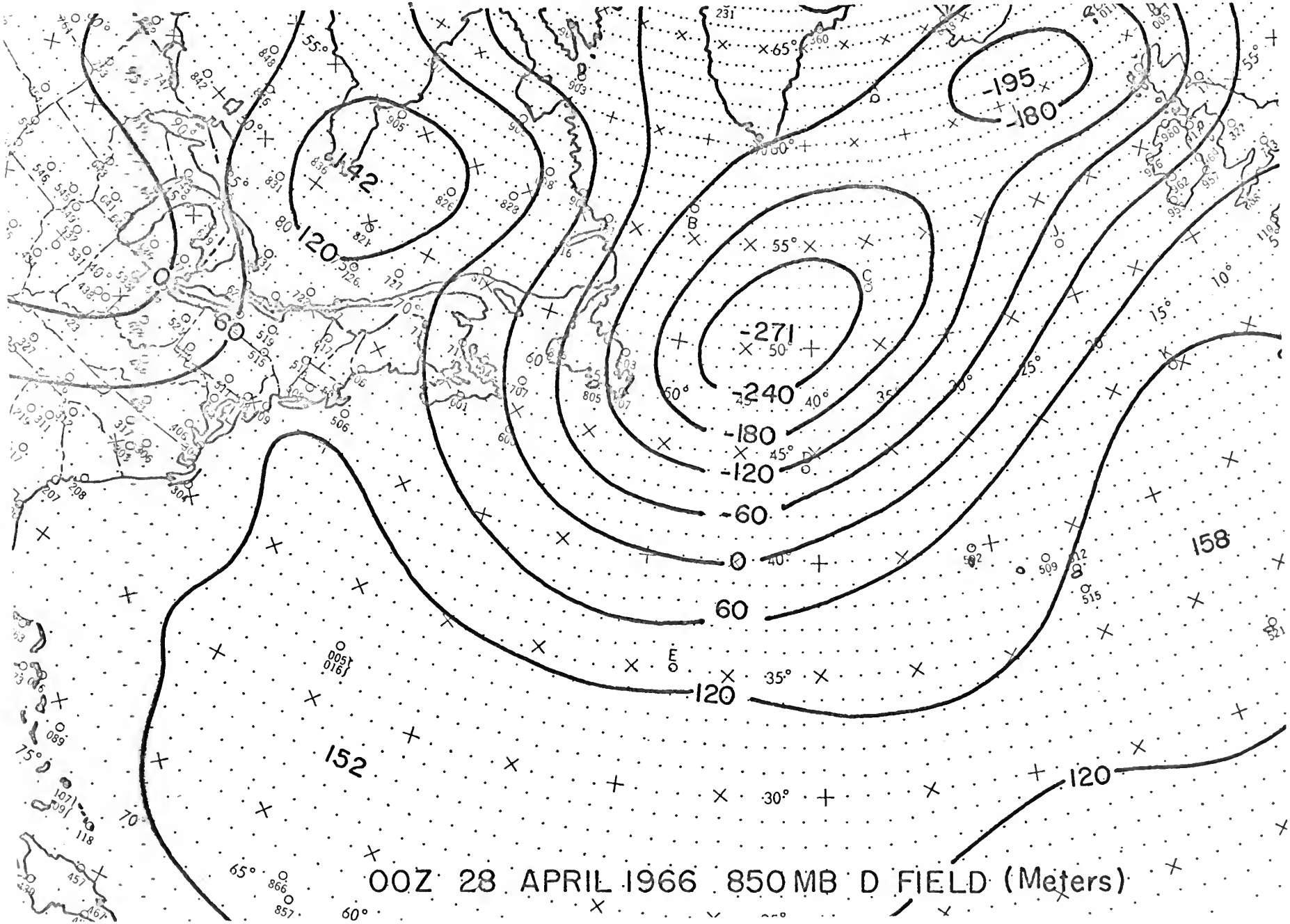
-195
-180
142
120
-271
-240
-180
-120
-60
0
60
120
158
152
120
00Z 28 APRIL 1966 850 MB D FIELD (Meters)

Figure 6

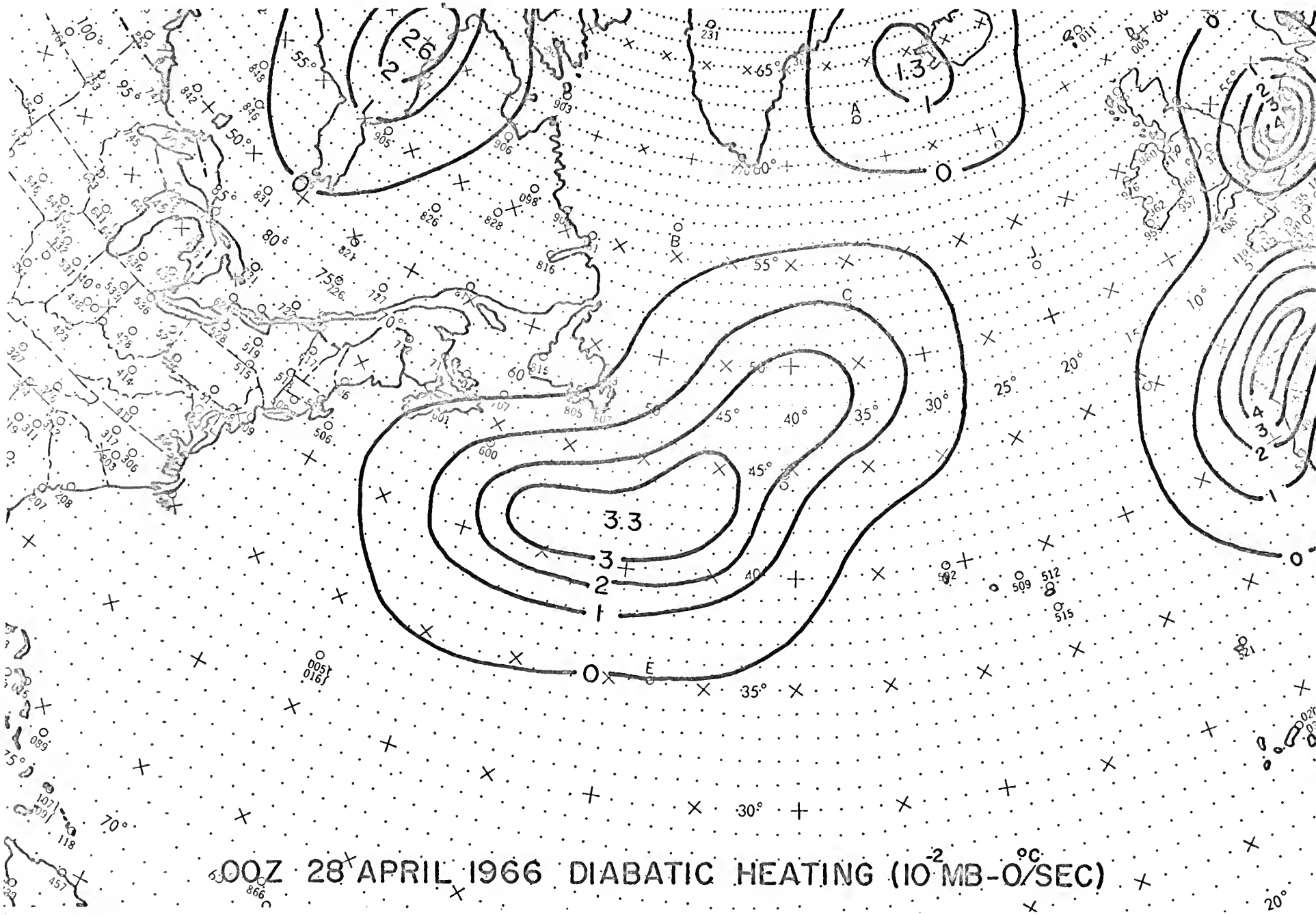

Figure 7

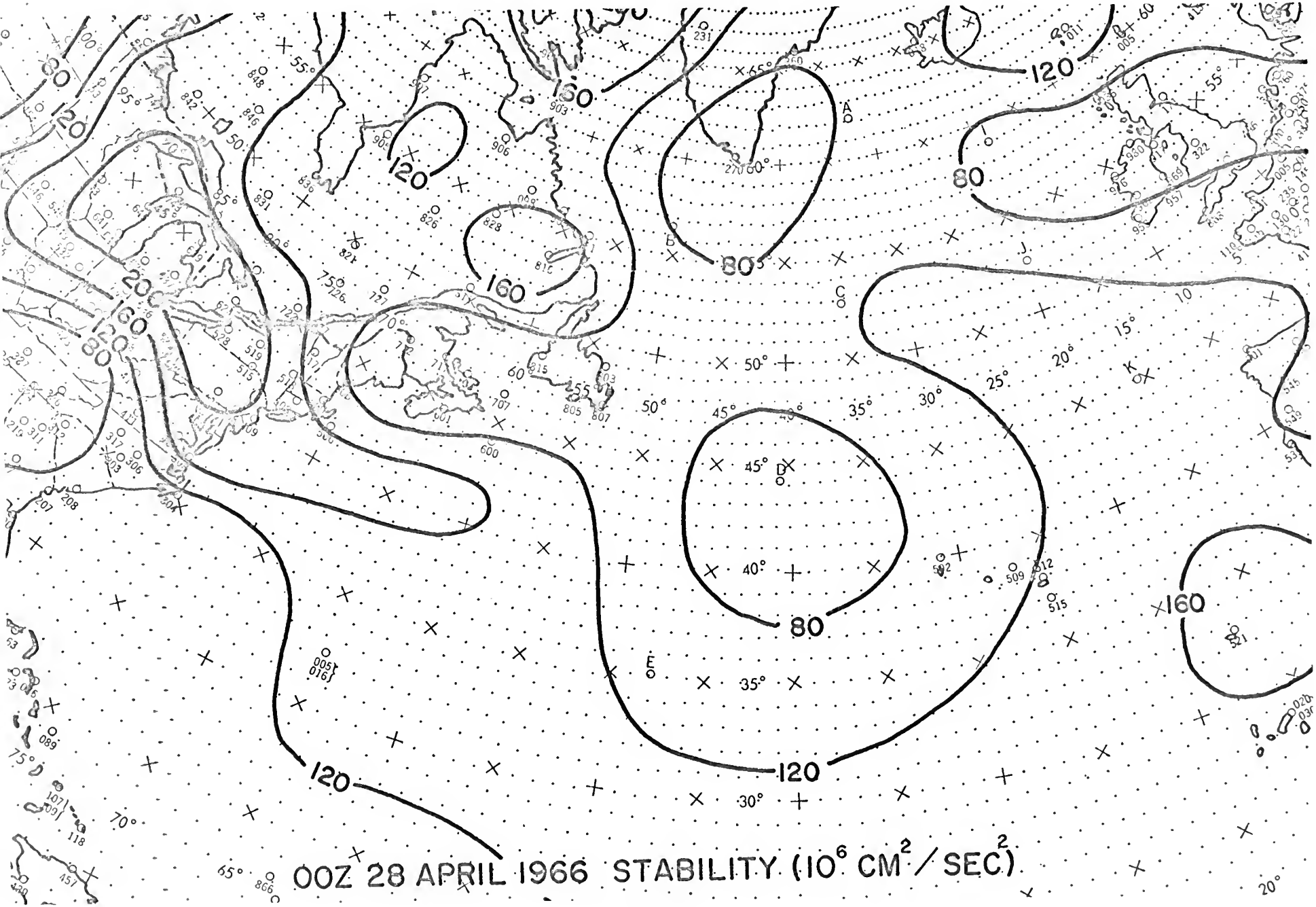

Figure 8

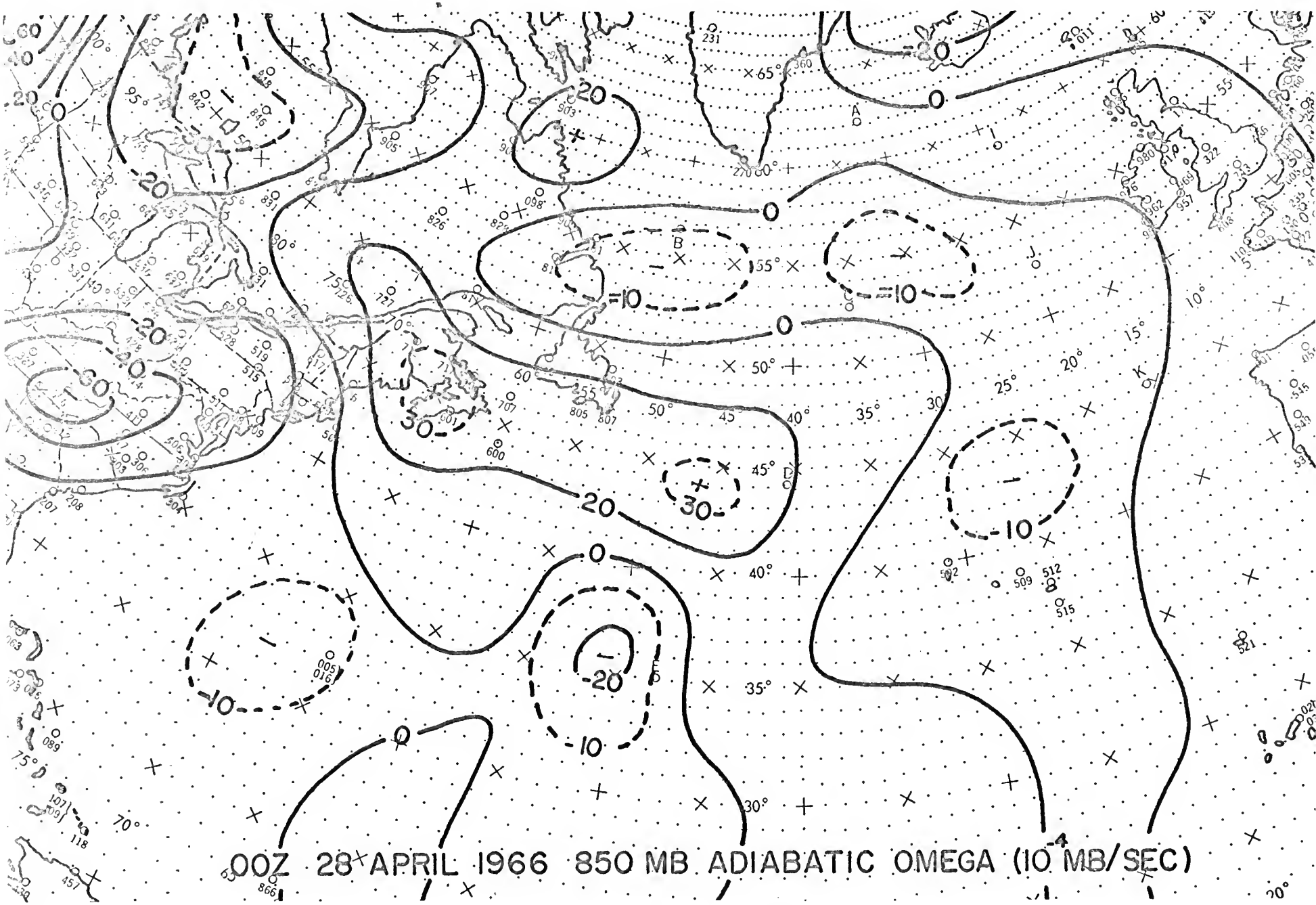

Figure 9

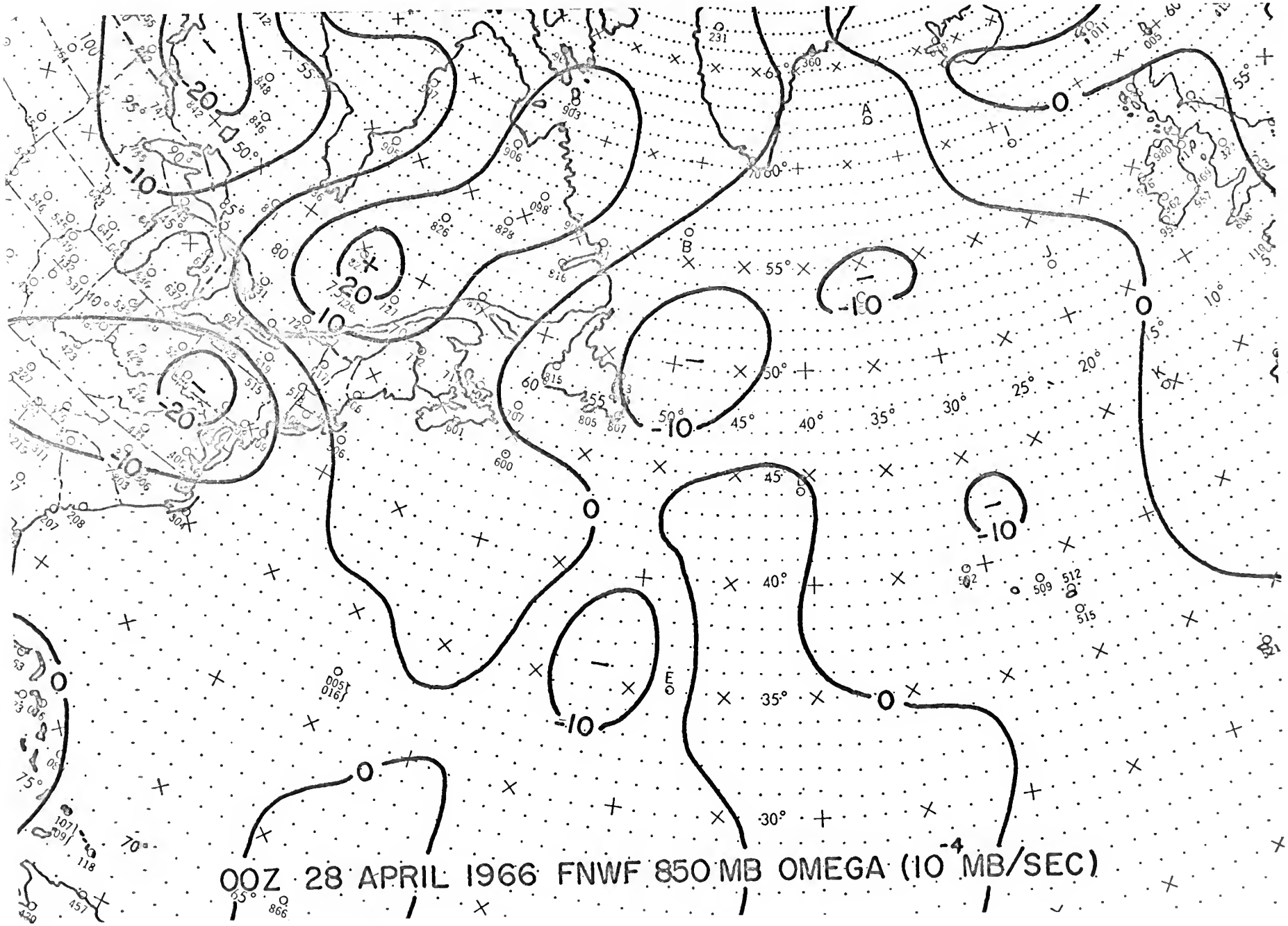

Figure 10

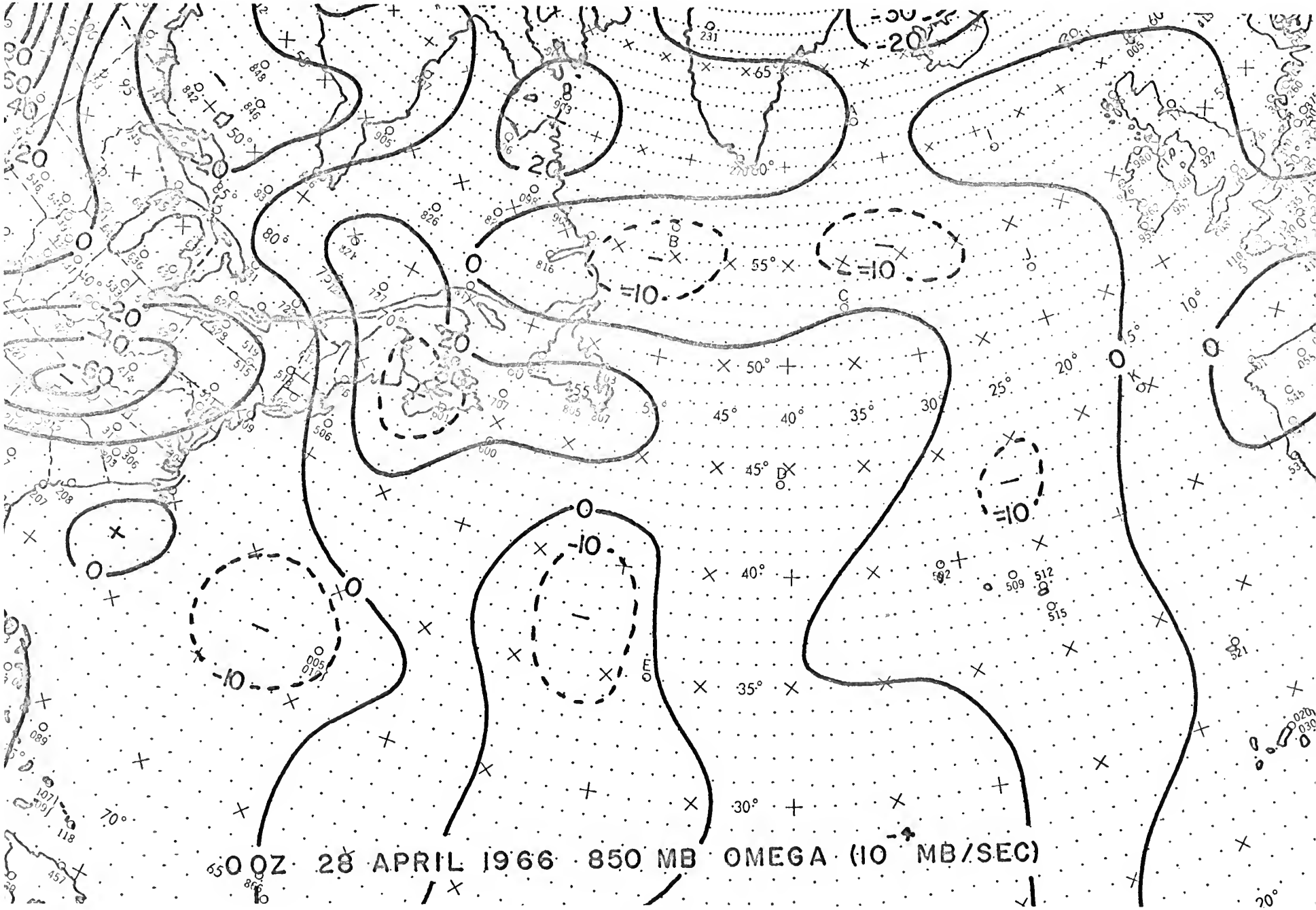

Figure 11

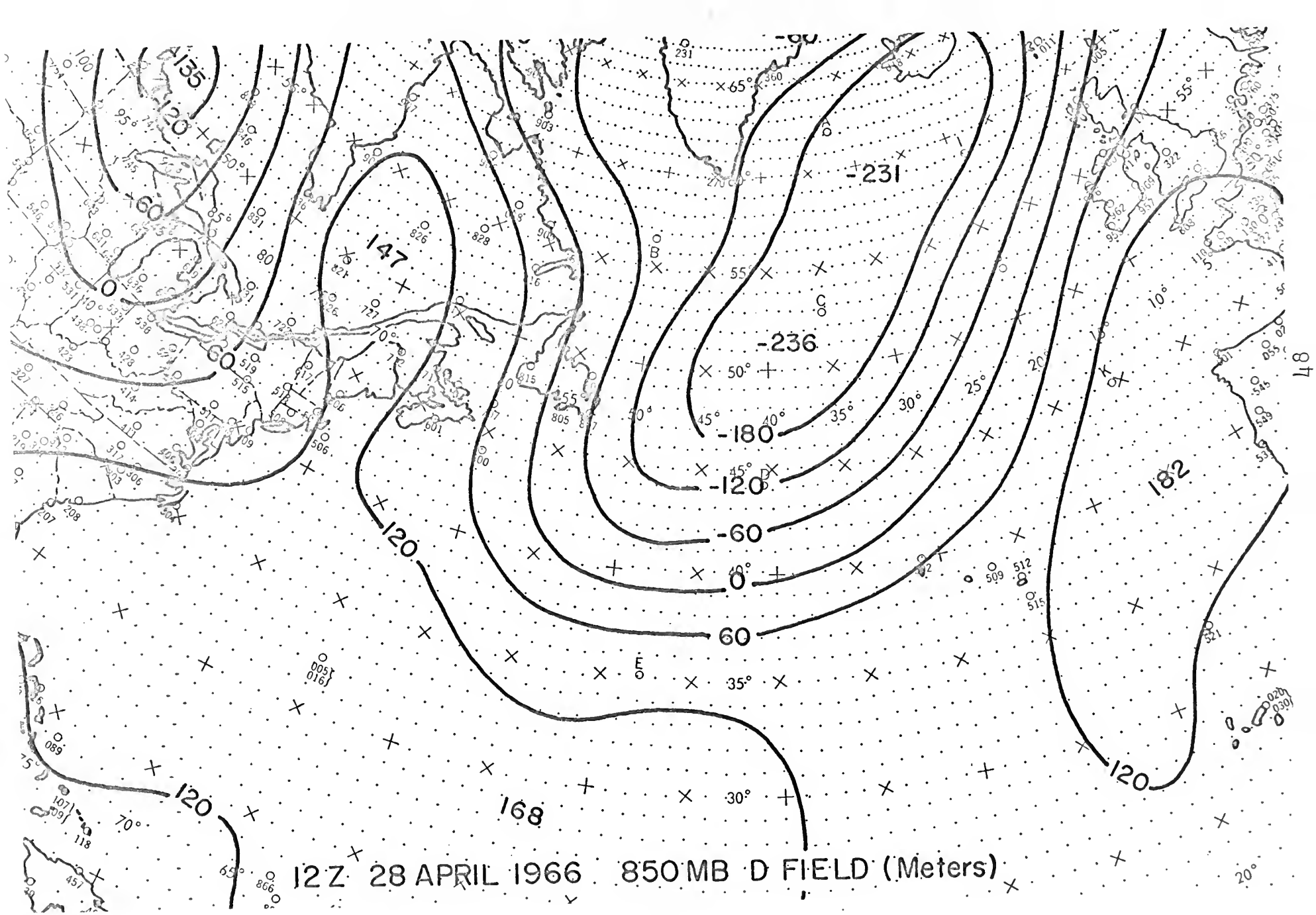
-90
-231
-236
-180
-120
-60
0
60
120
135
120
60
0
147
182
120
168
120
65°
55°
50°
45°
40°
35°
30°
25°
20°
10°
12Z 28 APRIL 1966 850MB D FIELD (Meters)

Figure 12

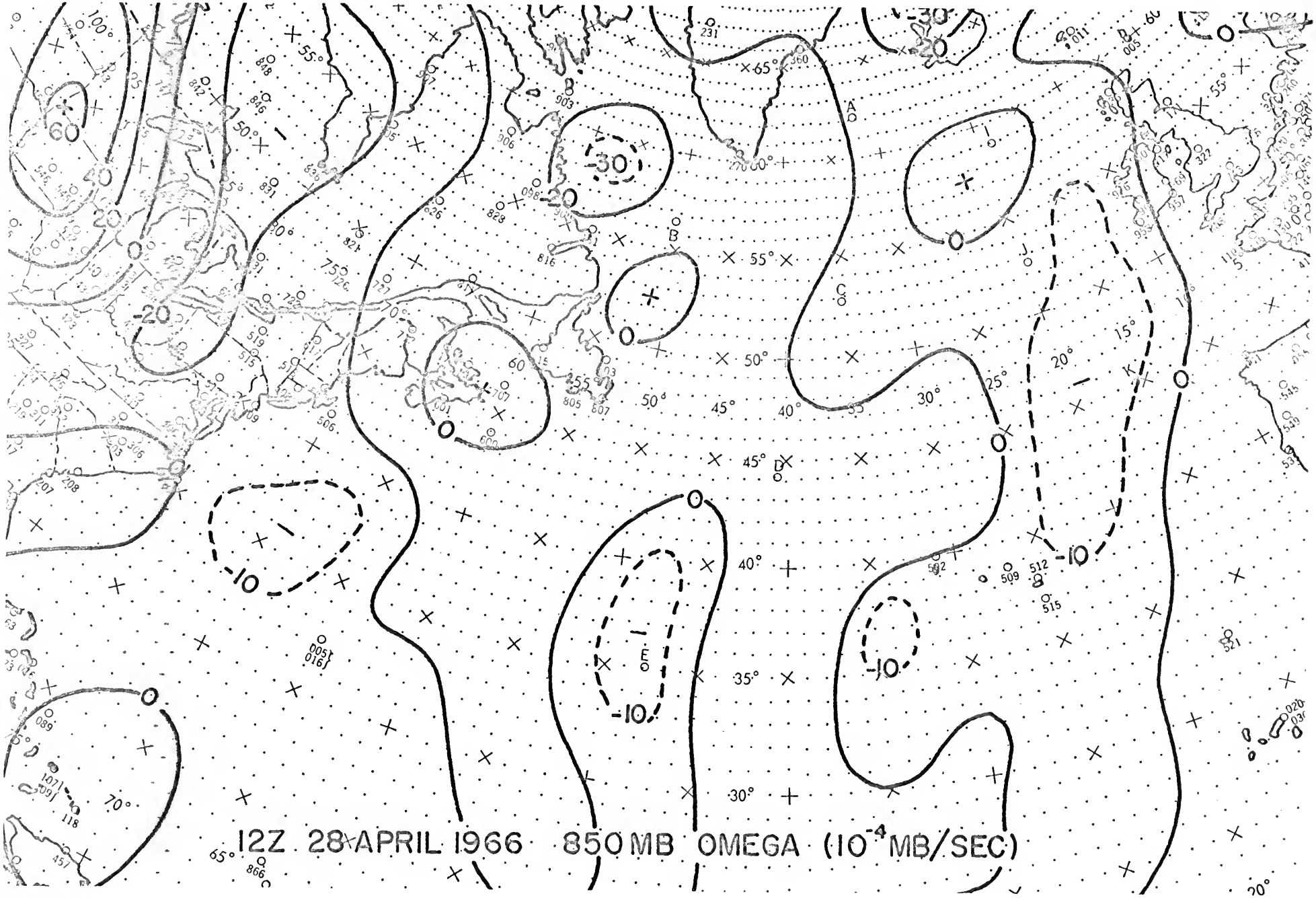

Figure 13

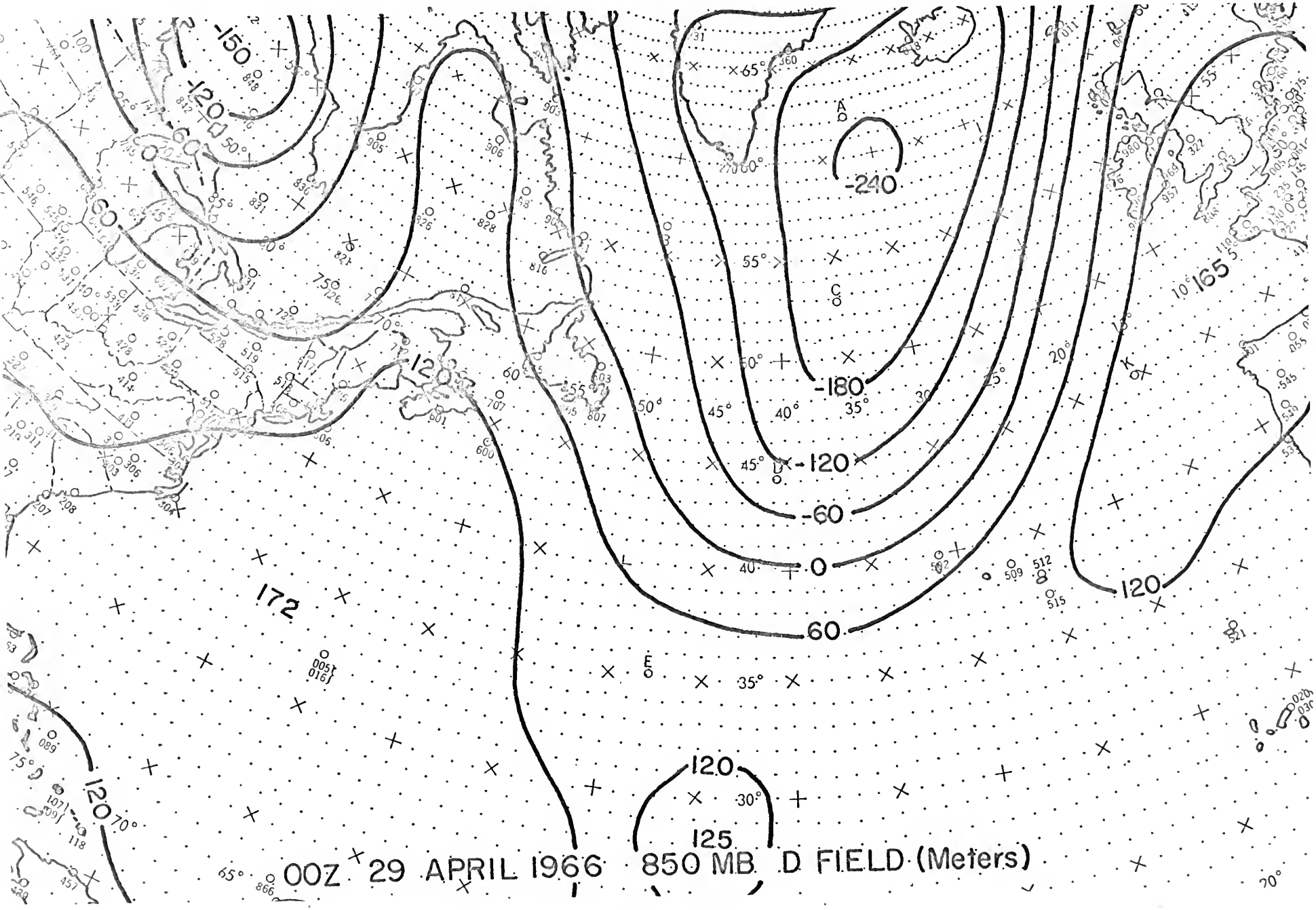

Figure 14

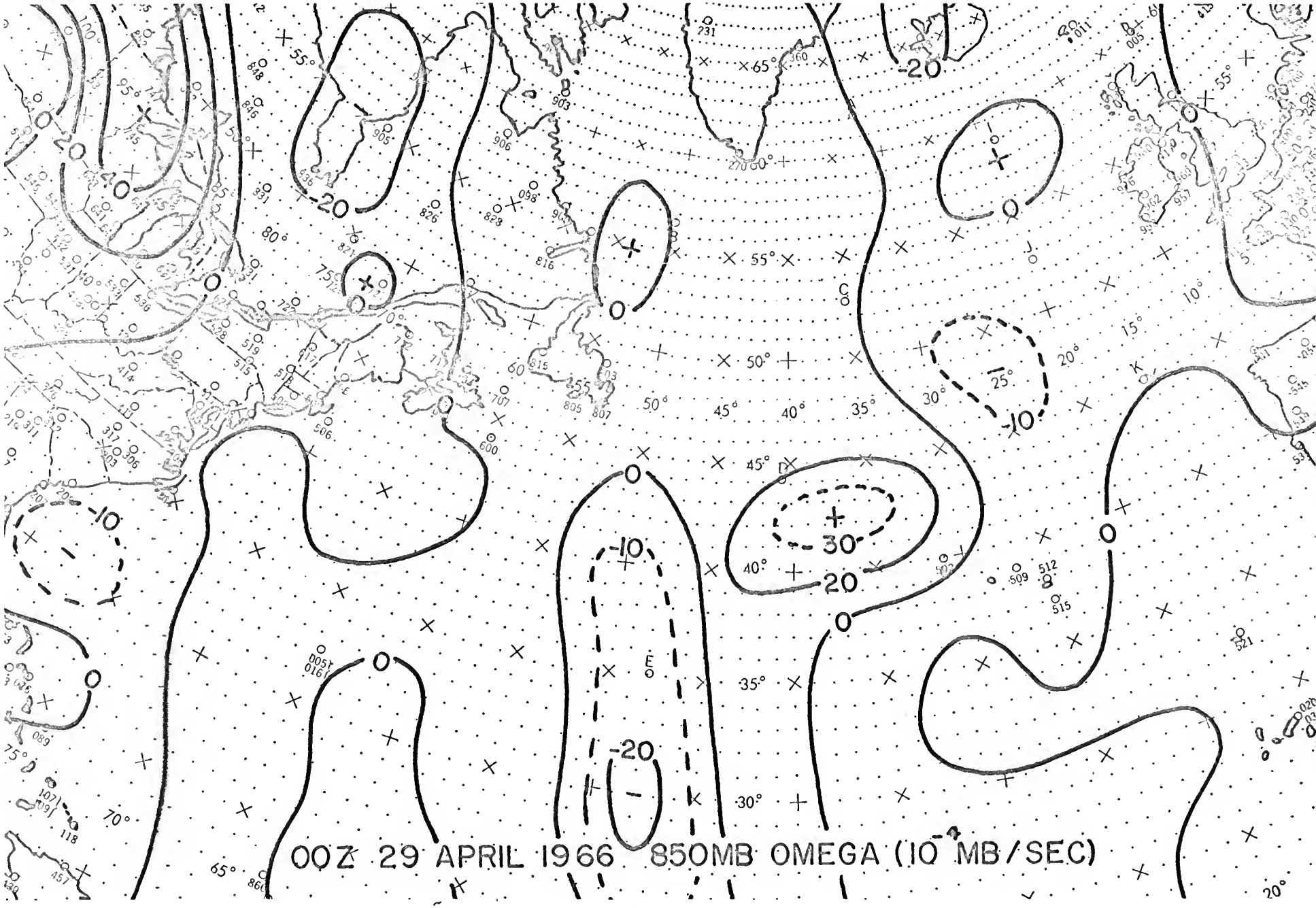

Figure 15

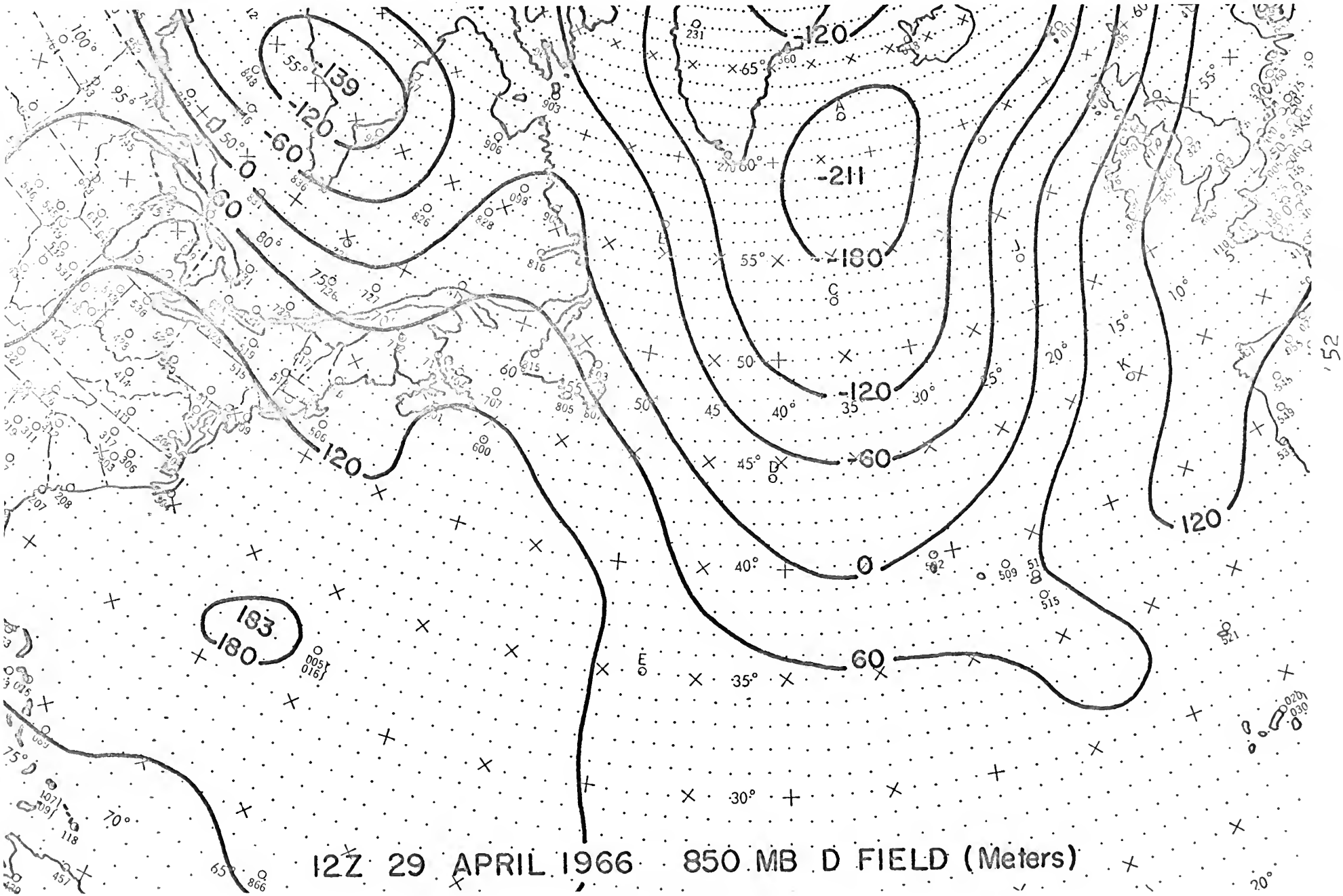
-120
-211
-180
-120
-60
0
60
120
-139
-120
-60
0
60
120
183
180
12Z 29 APRIL 1966 850 MB D FIELD (Meters)

Figure 16

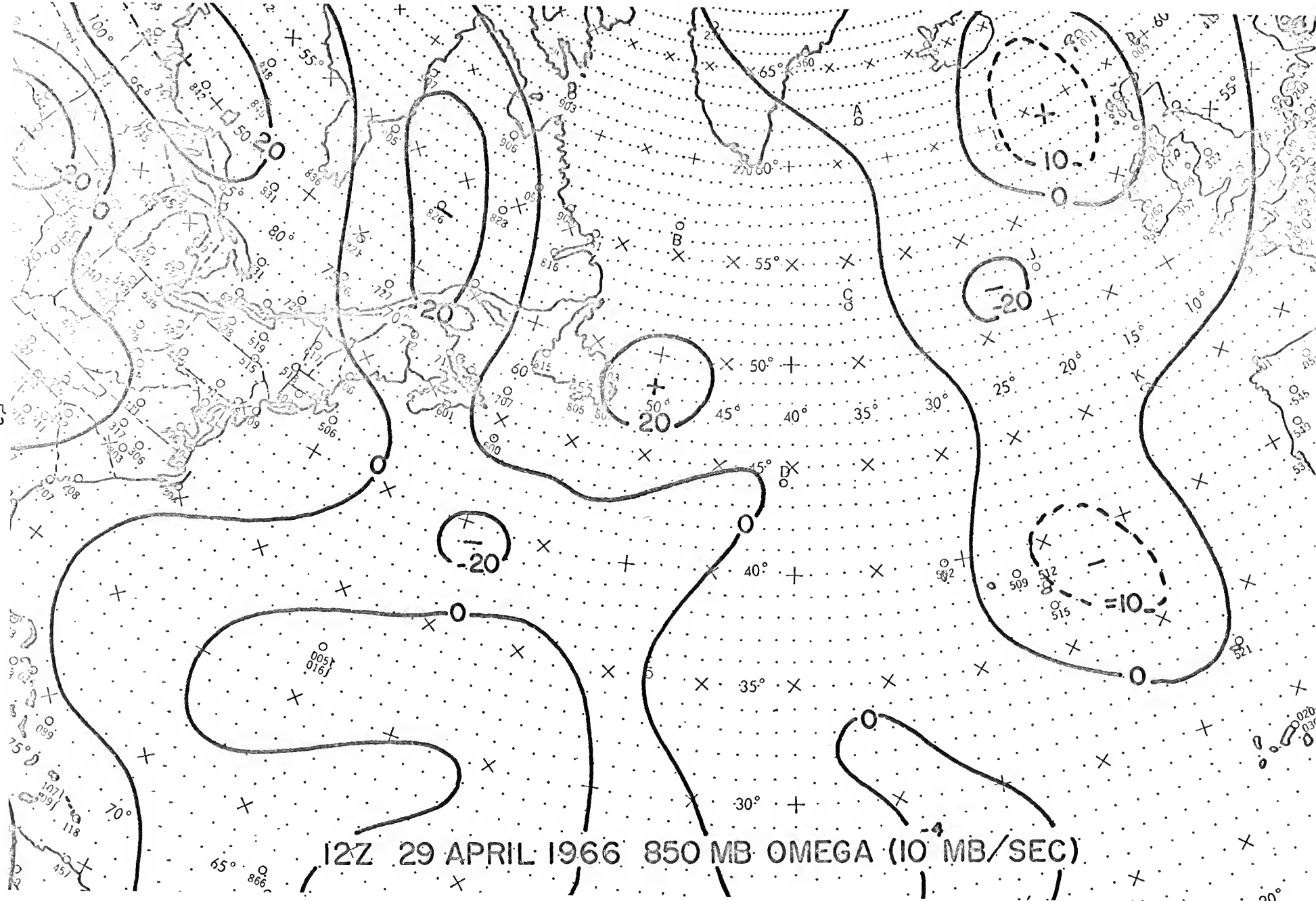

Figure 17

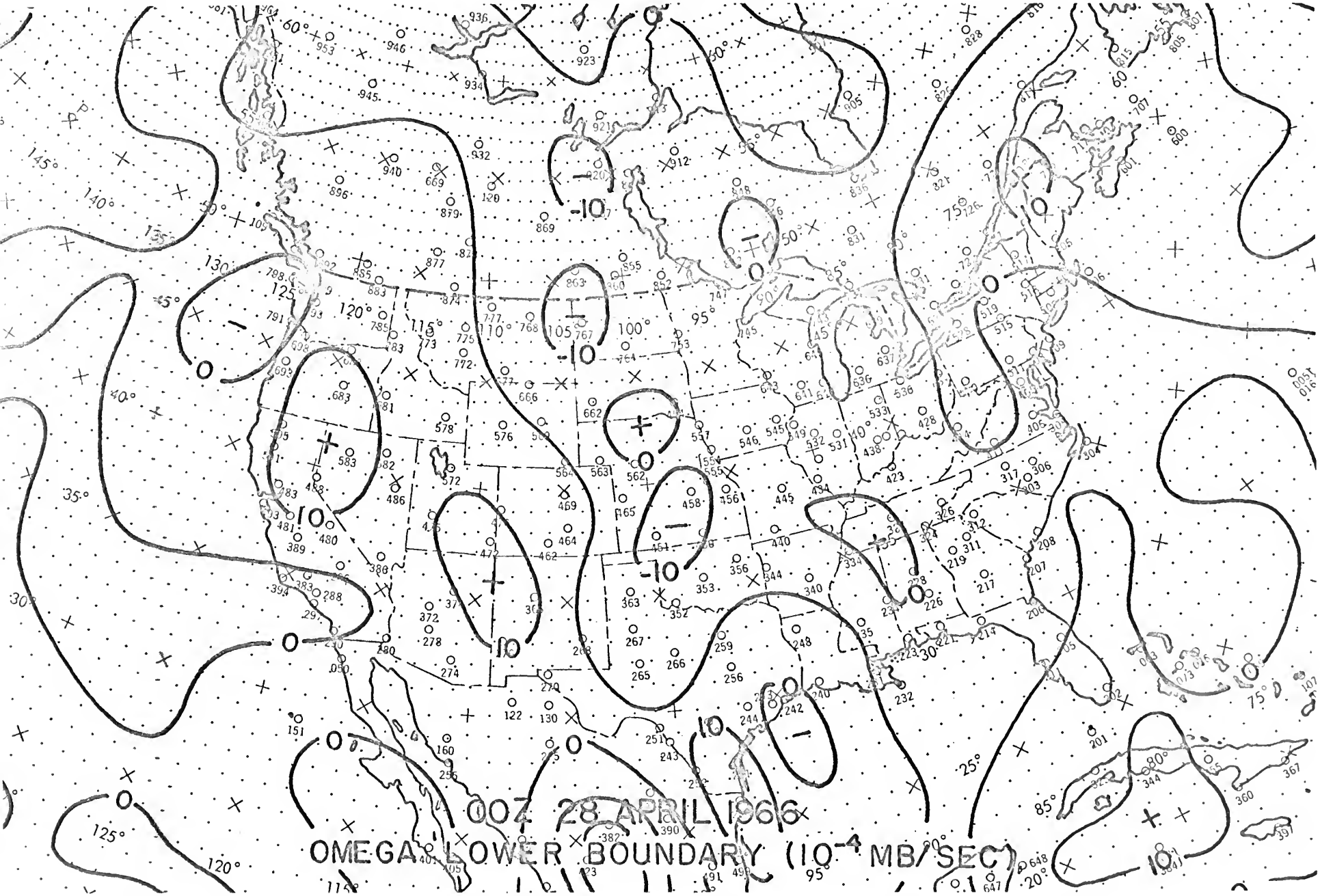

Figure 18

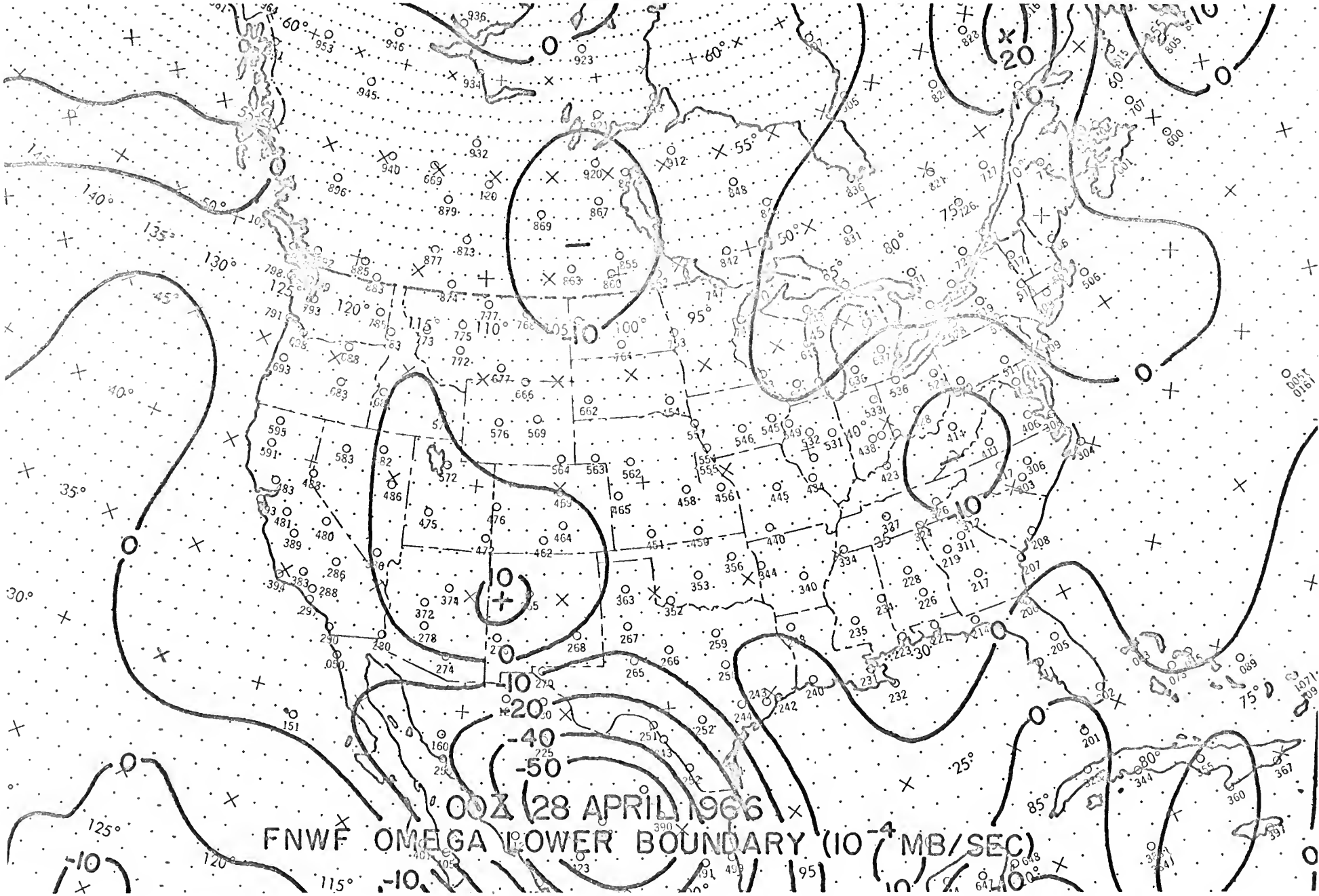

Figure 19

BIBLIOGRAPHY

1. Åmot, Audvin. On the Temperature Difference Between the Air and the Sea Surface and Its Applicability in the Practical Weather Analysis. Meteorolgiske Annaler, BD. 1, NR. 19, 1944.

2. Berkofski, L. and E. A. Bertoni. Mean Topographic Charts for the Entire Earth. Bulletin of the American Meteorological Society, 36, 1955, 350-354.

3. Blackadar, A. K. The Vertical Distribution of Wind and Turbulent Exchange in a Neutral Atmosphere. Journal of Geophysical Research, Vol. 67, No. 8, July, 1962.

4. Boyum, G. A Study of Evaporation and Heat Exchange Between the Sea Surface and the Atmosphere. Geofysiske Publikasjoner, Vol. XXII, No. 7, January, 1962

5. Burke, C. J. Transformation of Polar Continental Air to Polar Maritime Air. Journal of Meteorology, Vol. 2, No. 2, June, 1945

6. Carstensen, L. P. and T. Laevastu. FNWF Technical Note No. 17, April, 1966.

7. Cressman, G. P. Improved Terrain Effects in Barotropic Forecasts. Monthly Weather Review, 88, pp. 327-342, 1960.

8. Edson, H. Numerical Cloud and Icing Forecasts. Scientific Services Technical Note No. 13, Headquarters 3D Weather Wing, Scientific Services.

9. Haltiner, G. J., L. C. Clarke, and G. E. Lawniczak. Computation of the Large Scale Vertical Velocity. Journal of Applied Meteorology, Vol. 2, No. 2, pp. 242-259, April, 1963.

10. Haltiner, G. J. and F. L. Martin. Physical and Dynamical Meteorology. New York, McGraw-Hill, 1957.

11. Holl, M. M. J. P. Bibbo, and J. R. Clark. Linear Transforms for State-Parameter Structure, edition two, Meteorology International Technical Memorandum, No. 1, 1 October, 1963.

12. Laevastu, T. Factors Affecting the Temperature of the Surface Layer of the Sea. Societas Scientiarum Fennica, Helsinki, 1960

13. Lettau, H. H. Wind Profile, Surface Stress and Geostrophic Drag Coefficients in the Atmospheric Surface Layer. Advances in Geophysics, Vol. 6, pp. 241-257, Academic Press, New York, 1959.

14. Martin, F. L. Derivation of the Diabatic Heating Term. Unpublished Paper, 1966.

15. Mosby, H. The Sea-Surface and the Air. Scientific Results of the Norwegian Antarctic Expeditions 1927-1928, No. 10, Oslo, 1933.

16. Pedersen, K. An Experiment in Quantative Precipitation Forecasting with a Quasi-Geostrophic Model. University of Chicago Department of the Geophysical Sciences, Report No. 1, October, 1962.

17. Petterssen, S., D. L. Bradbury, and K. Pedersen. Heat Studies in Weather Analysis and Forecasting. Dept. of the Geophysical Sciences, University of Chicago, September, 1963.

18. Thompson, P. D. Numerical Weather Analysis and Prediction. New York, MacMillan, 1961.

INITIAL DISTRIBUTION LIST

		No. Copies
1.	Lt. P. S. Ferrentino 1807B Withington China Lake, Calif.	5
2.	F. L. Martin Environ. Sciences USN Postgraduate School Monterey, Calif.	6
3.	Library U. S. Naval Postgraduate School Monterey, California 93940	2
4.	Dept. of Meteorology & Oceanography U. S. Naval Postgraduate School Monterey, California 93940	1
5.	Defense Documentation Center Cameron Station Alexandria, Virginia 22314	20
6.	Office of the U. S. Naval Weather Service U. S. Naval Station (Washington Navy Yard Annex) Washington, D. C. 20390	1
7.	Chief of Naval Operations OP-09B7 Washington, D. C. 20350	1
8.	Officer in Charge Naval Weather Research Facility U. S. Naval Air Station, Bldg. R-48 Norfolk, Virginia 23511	1
9.	Commanding Officer FWC/JTWC COMNAVMAR FPO San Francisco, Calif. 96630	1
10.	Commanding Officer U. S. Fleet Weather Central, Kodiak FPO Seattle, Washington 98790	1
11.	Commanding Officer U. S. Fleet Weather Central, Pearl Harbor FPO San Francisco, California 96610	1

12.	Commanding Officer U. S. Fleet Weather Center, Rota FPO New York, New York 09540	1
13.	Commanding Officer Fleet Weather Central, Suitland Navy Department Washington, D. C. 20390	1
14.	Commanding Officer Fleet Weather Central U. S. Naval Air Station Alameda, California 94501	1
15.	Commanding Officer and Director Navy Electronics Laboratory Attn: Code 2230 San Diego, California 92152	1
16.	Officer in Charge U. S. Fleet Weather Facility, Argentia FPO New York, New York 09597	1
17.	Officer in Charge U. S. Fleet Weather Facility, Keflevik FPO New York, New York 09571	1
18.	Officer in Charge U. S. Fleet Weather Facility, Yokosuka FPO San Francisco, California 96662	1
19.	Officer in Charge U. S. Fleet Weather Facility, Sangley Point FPO San Francisco, California 96652	1
20.	Officer in Charge Fleet Weater Facility U. S. Naval Air Station San Diego, California 92135	1
21.	Officer in Charge Fleet Weather Facility U. S. NavalAir Station Quonset Point, Rhode Island 02819	1
22.	Officer in Charge Fleet Weather Facility Box 85 Naval Air Station Jacksonville, Florida 32212	1

23.	Officer in Charge Fleet Numerical Weather Facility U. S. Naval Postgraduate School Monterey, California 93940	2
24.	U. S. Naval War College Newport, Rhode Island 02844	1
25.	Director, Naval Research Laboratory Attn: Tech. Services Info. Officer Washington, D. C. 20390	1
26.	Office of Chief Signal Officer Research and Development Division Department of the Army Washington, D. C.	1
27.	Commander Air Force Cambridge Research Center Department of the Army Washington, D. C.	1
28.	Geophysics Research Directorate Air Force Cambridge Research Center Cambridge, Massachusetts	1
29.	Naval Air Technical Training Unit U. S. Naval Air Station Lakehurst, New Jersey 08733	1
30.	Program Director for Meteorology National Science Foundation Washington, D. C.	1
31.	Headquarters 2nd Weather Wing (MAC) United States Air Force APO #633 New York, New York	1
32.	American Meteorological Society 45 Beacon Street Boston, Massachusetts	1
33.	Commander, Air Weather Service Military Airlift Command U. S. Air Force Scott Air Force Base, Illinois 62226	2
34.	U. S. Department of Commerce Weather Bureau Washington, D. C.	2

35. Commandant of the Marine Corps — 1
Navy Department (Code DF)
Washington, D. C. 20380

36. Office of Naval Research — 1
Department of the Navy
Washington, D. C. 20360

37. U. S. Naval Oceanographic Office — 1
Attn: Division of Oceanography
Washington, D. C. 20390

38. Superintendent — 1
United States Naval Academy
Annapolis, Maryland 21402

39. Director — 1
Coast and Geodetic Survey
U. S. Department of Commerce
Attn: Office of Oceanography
Washington, D. C.

40. Office of Naval Research — 1
Department of the Navy
Attn: Geophysics Branch (Code 416)
Washington, D. C. 20360

41. Office of Naval Research — 1
Department of the Navy
Attn: Director, Surface and Amphibious
Programs (Code 463)

42. Program Director Oceanography — 1
National Science Foundation
Washington, D. C.

43. Council on Wave Research — 1
Department of Civil Engineering
University of California
Berkeley, California

44. Director — 1
National Oceanographic Data Center
Washington, D. C.

45. Director — 1
Woods Hole Oceanographic Institution
Woods Hole, Massachusetts 02543

46. Chairman — 1
Department of Meteorology & Oceanography
New York University
University Heights, Bronx
New York, New York

47. Director 1
Scripps Institution of Oceanography
University of California, San Diego
La Jolla, California

48. Bingham Oceanographic Laboratories 1
Yale University
New Haven, Connecticut

49. Director, Institute of Marine Science 1
University of Miami
#1 Rickenbacker Causeway
Virginia Key
Miami, Florida

50. Department of Meteorology & Oceanography 1
Chairman
University of Hawaii
Honolulu, Hawaii

51. Director 1
Lamont Geological Observatory
Torrey Cliff
Palisades, New York

52. Chairman, Department of Oceanography 1
Oregon State University
Corvallis, Oregon 97331

53. Chairman, Department of Oceanography 1
University of Rhode Island
Kingston, Rhode Island

54. Texas A & M University 1
Chairman, Department of Oceanography
College Station, Texas 77843

55. Executive Officer 1
Department of Oceanography
University of Washington
Seattle, Washington 98105

56. National Research Council 1
2101 Constitution Avenue
Washington, D. C.
Attn: Committee on Undersea Warfare

57. Chairman 1
Department of Oceanography
The Johns Hopkins University
Baltimore, Maryland

58.	Library Florida Atlantic University Boca Raton, Florida	1
59.	Department of Meteorology University of California Los Angeles, California	1
60.	Department of the Geophysical Sciences University of Chicago Chicago, Illinois	1
61.	Department of Atmospheric Science Colorado State University Fort Collins, Colorado	1
62.	Department of Engineering Mechanics University of Michigan Ann Arbor, Michigan	1
63.	School of Physics University of Minnesota Minneapolis, Minnesota	1
64.	Department of Meteorology University of Utah Salt Lake City, Utah	1
65.	National Center for Atmospheric Research Boulder Colorado	1
66.	Department of Meteorology and Climatology University of Washington Seattle, Washington 98105	1
70.	Department of Meteorology University of Wisconsin Madison, Wisconsin	1
71.	Department of Meteorology Florida State University Tallahassee, Florida	1
72.	Department of Meteorology Massachusetts Institute of Technology Cambridge, Massachusetts 02139	1
73.	Department of Meteorology Pennsylvania State University University Park, Pennsylvania	1

74.	Hawaii Institute of Geophysics University of Hawaii Honolulu, Hawaii	1
75.	University of Oklahoma Research Intitute Norman, Oklahoma	1
76.	Atmospheric Science Branch Science Research Institute Oregon State College Corvallis, Oregon	1
77.	The University of Texas Electrical Engineering Research Laboratory Engineering Science Bldg. 631A University Station Austin, Texas 78712	1
78.	Department of Meteorology Texas A & M University College Station, Texas 77843	1
79.	Lamont Geological Observatory Columbia University Palisades, New York	1
80.	Division of Engineering and Applied Physics Room 206, Pierce Hall Harvard University Cambridge, Massachusetts	1
81.	Department of Mechanics The Johns Hopkins University Baltimore, Maryland	1
82.	University of California E. O. Lawrence Radiation Laboratory Livermore, California	1
83.	Department of Astrophsics and Atmospheric Physics University of Colorado Boulder, Colorado	1
84.	Weather Dynamics Group Aerophysics Laboratory Stanford Research Institute Menlo Park, California	1

85. Meteorology International, Inc. 1
P. O. Box 1364
Monterey, California 93940

86. The Travelers Research Center, Inc. 1
650 Main Street
Hartford, Connecticut

87. United Air Lines 1
Director of Meteorology
P. O. Box 8800
Chicago, Illinois

88. Department of Meteorology 1
University of Melbourne
Grattan Street
Parkville, Victoria
Australia

89. Bureau of Meteorology 1
Department of the Interior
Victoria and Drummond Streets
Carlton, Victoria
Australia

90. International Antarctic Analysis Centre 1
468 Lonsdale Street
Melbourne, Victoria
Australia

91. Department of Meteorology 1
McGill University
Montreal, Canada

92. Central Analysis Office 1
Meteorological Branch
Regional Adm. Building
Inter. Airport
Dorval, Quebec, Canada

93. Meteorological Office 1
315 Bloor Street West
Toronto 5, Ontario, Canada

94. Department of Meteorology 1
University of Copenhagen
Copenhagen, Denmark

95. Institute of Meteorology 1
University of Helsinki
Helsinki - Porthania, Finland

96. Institut fur Theoretische Meteorologie 1
Freie Universitat Berlin
Berlin-Dahlem
Thiel-allee 49
Federal Republic of Germany

97. Meteorological Institute 1
University of Thessaloniki
Thessaloniki, Greece

98. Meteorological Service 1
44, Upper O'Connell Street
Dublin 1, Ireland

99. Department of Meteorology 1
The Hebrew University
Jerusalem, Isreal

100. Geophysical Institute 1
Tokyo University
Bunkyo-ku
Tokyo, Japan

101. Meteorological Research Institute 1
Kyoto University
Kyoto, Japan

102. Department of Astronomy and Meteorology 1
College of Liberal Arts and Sciences
Seoul National University
Ibng Soong Dong, Chong No Ku
Seoul, Korea

103. Central Meteorological Office 1
I Song Wul Dong, Sudaemon Ku
Seoul, Korea

104. Department of Meteorology 1
Instituto de Geofisica
Universidad Nacional de Mexico
Mexico 20, D. F., Mexico

105. New Zealand Meteorological Service 1
P. O. Box 722
Wellington, G. E. New Zealand

106. Institutt for Teoretisk Meteorologi 1
University of Oslo
Blindern, Oslo, Norway

107.	Institute of Geophysics University of Bergen Bergen, Norway	1
108.	Pakistan Meteorological Department Institute of Meteorology and Geophysics Karachi, Pakistan	1
109.	Royal Swedish Air Force M. V. C. Stockholm 80, Sweden	1
110.	Department of Meteorology Imperial College of Science South Kensington London S. W. 7, United Kingdom	1
111.	Meteorological Office London R. Bracknell Berkshire, United Kingdom	1
112.	National Research Institute for Mathematical Sciences C. S. I. R. P. O. Box 395 Pretoria, Union of South Africa	1
113.	Commonwealth Scientific and Industrial Research Organization 314 Albert Street East Melbourne, C. 2, Victoria	1
114.	Director Pacific Oceanographic Group Nanaimo, British Columbia Canada	1
115.	Ocean Research Institute University of Tokyo Tokyo, Japan	1

DOCUMENT CONTROL DATA - R&D

(Security classification of title, body of abstract and indexing annotation must be entered when the overall report is classified)

1. ORIGINATING ACTIVITY *(Corporate author)*
U. S. NAVAL POSTGRADUATE SCHOOL

2a. REPORT SECURITY CLASSIFICATION
UNCLASSIFIED

2b. GROUP

3. REPORT TITLE
A TWO-DIMENSIONAL OMEGA EQUATION FOR THE 1000-700 MB LAYER WITH DIABATIC HEATING

4. DESCRIPTIVE NOTES *(Type of report and inclusive dates)*
MASTER OF SCIENCE THESIS (METEOROLOGY)

5. AUTHOR(S) *(Last name, first name, initial)*
FERRENTINO, PETER S.
LIEUTENANT, U. S. NAVY

6. REPORT DATE	7a. TOTAL NO. OF PAGES	7b. NO. OF REFS
1 May 1966	66	18

8a. CONTRACT OR GRANT NO.	9a. ORIGINATOR'S REPORT NUMBER(S)
b. PROJECT NO.	
c.	9b. OTHER REPORT NO(S) *(Any other numbers that may be assigned this report)*
d.	

10. AVAILABILITY/LIMITATION NOTICES
[redacted] ORR 9/15/69
This document has been approved for public release and sale; its distribution is unlimited.

11. SUPPLEMENTARY NOTES	12. SPONSORING MILITARY ACTIVITY
	Chief of Naval Operations(OP-09B7) Department of the Navy Washington, D. C. 20360

13. ABSTRACT

A two-dimensional omega equation is derived by combination of the vorticity and thermodynamic equations. The desired omega is then taken to be the logarithmic average in the 1000-700 mb layer. A diabatic term, after Laevastu, for oceanic areas only is included to deduce the empirical temperature and vapor-pressure changes associated with sensible and latent heating in the maritime layers. Over both continental and oceanic areas a frictional vorticity sink is included in order that excessive energy cannot be generated over the ocean. Among other novel features is the use of the Holl static-stability parameter which affords vertical consistency in the analyses prepared by Fleet Numerical Weather Facility.

DD FORM 1 JAN 64 1473

14. KEY WORDS	LINK A		LINK B		LINK C	
	ROLE	WT	ROLE	WT	ROLE	WT
LAYER-MEAN OMEGA						
OMEGA EQUATION						
VERTICAL MOTION						
DIABATIC HEATING						

INSTRUCTIONS

1. ORIGINATING ACTIVITY: Enter the name and address of the contractor, subcontractor, grantee, Department of Defense activity or other organization *(corporate author)* issuing the report.

2a. REPORT SECURITY CLASSIFICATION: Enter the overall security classification of the report. Indicate whether "Restricted Data" is included. Marking is to be in accordance with appropriate security regulations.

2b. GROUP: Automatic downgrading is specified in DoD Directive 5200.10 and Armed Forces Industrial Manual. Enter the group number. Also, when applicable, show that optional markings have been used for Group 3 and Group 4 as authorized.

3. REPORT TITLE: Enter the complete report title in all capital letters. Titles in all cases should be unclassified. If a meaningful title cannot be selected without classification, show title classification in all capitals in parenthesis immediately following the title.

4. DESCRIPTIVE NOTES: If appropriate, enter the type of report, e.g., interim, progress, summary, annual, or final. Give the inclusive dates when a specific reporting period is covered.

5. AUTHOR(S): Enter the name(s) of author(s) as shown on or in the report. Enter last name, first name, middle initial. If military, show rank and branch of service. The name of the principal author is an absolute minimum requirement.

6. REPORT DATE: Enter the date of the report as day, month, year; or month, year. If more than one date appears on the report, use date of publication.

7a. TOTAL NUMBER OF PAGES: The total page count should follow normal pagination procedures, i.e., enter the number of pages containing information.

7b. NUMBER OF REFERENCES: Enter the total number of references cited in the report.

8a. CONTRACT OR GRANT NUMBER: If appropriate, enter the applicable number of the contract or grant under which the report was written.

8b, 8c, & 8d. PROJECT NUMBER: Enter the appropriate military department identification, such as project number, subproject number, system numbers, task number, etc.

9a. ORIGINATOR'S REPORT NUMBER(S): Enter the official report number by which the document will be identified and controlled by the originating activity. This number must be unique to this report.

9b. OTHER REPORT NUMBER(S): If the report has been assigned any other report numbers *(either by the originator or by the sponsor)*, also enter this number(s).

10. AVAILABILITY/LIMITATION NOTICES: Enter any limitations on further dissemination of the report, other than those imposed by security classification, using standard statements such as:

(1) "Qualified requesters may obtain copies of this report from DDC."

(2) "Foreign announcement and dissemination of this report by DDC is not authorized."

(3) "U. S. Government agencies may obtain copies of this report directly from DDC. Other qualified DDC users shall request through _____."

(4) "U. S. military agencies may obtain copies of this report directly from DDC. Other qualified users shall request through _____."

(5) "All distribution of this report is controlled. Qualified DDC users shall request through _____."

If the report has been furnished to the Office of Technical Services, Department of Commerce, for sale to the public, indicate this fact and enter the price, if known.

11. SUPPLEMENTARY NOTES: Use for additional explanatory notes.

12. SPONSORING MILITARY ACTIVITY: Enter the name of the departmental project office or laboratory sponsoring *(paying for)* the research and development. Include address.

13. ABSTRACT: Enter an abstract giving a brief and factual summary of the document indicative of the report, even though it may also appear elsewhere in the body of the technical report. If additional space is required, a continuation sheet shall be attached.

It is highly desirable that the abstract of classified reports be unclassified. Each paragraph of the abstract shall end with an indication of the military security classification of the information in the paragraph, represented as *(TS), (S), (C), or (U)*.

There is no limitation on the length of the abstract. However, the suggested length is from 150 to 225 words.

14. KEY WORDS: Key words are technically meaningful terms or short phrases that characterize a report and may be used as index entries for cataloging the report. Key words must be selected so that no security classification is required. Identifiers, such as equipment model designation, trade name, military project code name, geographic location, may be used as key words but will be followed by an indication of technical context. The assignment of links, roles, and weights is optional.